

# COUPLED LOGISTIC MAP: A REVIEW AND NUMERICAL FACTS

NEPTALÍ ROMERO, JESÚS SILVA, AND RAMÓN VIVAS

ABSTRACT. This paper has a double goal, the first one is to make a slight survey of some theoretical results about the existence of positively invariant curves that allow to describe important properties of the set of bounded orbits and its boundary in the context of coupled logistic map. The second goal, in the same context, is to show a collection of figures obtained from computational simulation that reveal the complexity of that dynamical systems.

## 1. INTRODUCTION

Since a few decades ago coupled map lattices have had special interest for physicists and scientists working in nonlinear pure and applied mathematics. The main reason for considering this type of dynamical systems is that they allow to describe time evolution of reaction-diffusion systems, population dynamics and a huge variety of important problems in several disciplines as physics, chemistry, economy and even sociology. One of the most popular coupled map lattices is the so-called *coupled logistic map* (on two sides):

$$(1.1) \quad F_{\mu,\epsilon}(x, y) = ((1 - \epsilon)f_\mu(x) + \epsilon f_\mu(y), (1 - \epsilon)f_\mu(y) + \epsilon f_\mu(x)),$$

where  $x, y \in \mathbb{R}$ ,  $f_\mu : \mathbb{R} \rightarrow \mathbb{R}$ , with  $f_\mu(t) = \mu t(1 - t)$  is the logistic map and  $\epsilon$  is the coupling strength. This two-parameter family is a singular class of coupled map lattices, it was introduced in independent works by Ian Frøyland [7], Kunihiro Kaneko [9], Raymond Kapral and Sergey Kuznetsov; see [2], [11]. These kind of discrete dynamical systems have been intensively used to model a wide number of spatio-temporal phenomena in extended systems; see for example [10].

Much of the numerical and theoretical studies of (1.1) obey certain physical interpretations under the following restrictions:  $0 \leq x, y \leq 1$ ,  $1 < \mu \leq 4$  and  $0 < \epsilon < 1$ . In this setting several numerical reports on the dynamics of (1.1) are well known, cf. [11] where an important survey on the subject is discussed; see also [4], [5] and [6] where some theoretical results are described.

In this paper we do not consider restrictions on the state space, that is  $x, y \in \mathbb{R}$ ; in addition we assume  $\mu > 1$  and  $\epsilon > 0$ . Although it is possible that there are no physical interpretations, these considerations seem interesting from the mathematical point of view. The principal aim in this paper is to report some computer simulations that could lead to theoretically prove some phenomena that occur, or

---

2010 *Mathematics Subject Classification.* 37C05, 37D99.

*Key words and phrases.* logistic map, coupled logistic map.

may be involved, in the fractalization of the basin of attraction of infinity, which is an attractor for the family  $F_{\mu,\epsilon}$ . Despite the fact that in the study of complicated chaotic behaviors, even in very simple dynamical systems, the numerical experimentation and their interpretations are not conclusive, they constitute an important support for a further analytical examination.

For the purpose of this paper we have taken as starting point some results in [17] and [18], especially those related to the existence of invariant Jordan curves having direct relationship with the set of points with bounded orbit; this will be recalled in next section. In Section 3 we show some computational simulations experiments followed by some interpretations.

## 2. THE STARTING POINT

We begin with some comments about the parameter space  $(\mu, \epsilon)$ . First we recall that:  $F_{\mu,\epsilon}$  and  $F_{2-\mu,\epsilon}$  are topologically conjugated when  $0 < \mu < 1$ , and the self-maps  $F_{\mu,\epsilon}$  and  $F_{\mu,1-\epsilon}$  are dynamically equivalents; see [17, Section 2]. On the other hand:  $F_{0,\epsilon}$  is constant,  $F_{\mu,0}$  maps  $\mathbb{R}^2$  into the diagonal and the dynamics of  $F_{1,\epsilon}$  is just simple: every point with bounded orbit has as  $\omega$ -limit set the origin (cf. Corollary 2.1 of [18]). After these facts we fix our attention on

$$\epsilon \in (-\infty, 0) \cup (0, 1/2) \text{ and } \mu > 1.$$

We say that the coupled logistic map  $F_{\mu,\epsilon}$  has *small strength* when  $\epsilon \in (0, 1/2)$ , and it has *large strength* if  $\epsilon \in (-\infty, 0)$ . Regardless of strength type, there are some common dynamical properties; we refer to [18] and [17] for their proofs:

- There are always two fixed points:  $O = (0, 0)$  and  $P_\mu = \left(\frac{\mu-1}{\mu}, \frac{\mu-1}{\mu}\right)$ , the nature of these points depends on  $\mu$  and  $\epsilon$ . Two other fixed points appear in a certain region of the parameter space  $(\mu, \epsilon)$ , although these points have the same algebraic expression for the different strengths:  $R(p_{\mu,\epsilon})$  and  $p_{\mu,\epsilon} = (p_-, p_+)$ , where  $R$  is the reflection  $R(x, y) = (y, x)$  and

$$p_\pm = \frac{k\mu \pm \sqrt{2(\mu-1)\mu k - \mu^2 k^2}}{2\mu} \text{ and } k = 1 - \frac{1}{\mu(1-2\epsilon)},$$

they appear through a pitchfork bifurcation for the fixed points  $O$  (small strength) and  $P_\mu$  (large strength).

- The infinity is always an attractor; that is, there exists a compact neighborhood whose complement  $U$  is positively invariant under  $F_{\mu,\epsilon}$  (i.e.  $F_{\mu,\epsilon}(U^c) \subset U^c$ ) and  $\|F_{\mu,\epsilon}^k(z)\| \rightarrow +\infty$  as  $k \rightarrow +\infty$  for all  $z \in U^c$ . It is easy to see that if  $C$  is the circle given by  $x^2 + y^2 = x + y$ , then the closed disk with boundary  $C$  takes the role of the set  $U$  above. Thus, if  $ext C$  denotes the unbounded component of the complement of  $C$ , then it is contained in

$$B_\infty(F_{\mu,\epsilon}) = \{z \in \mathbb{R}^2 : \lim_{k \rightarrow +\infty} \|F_{\mu,\epsilon}^k(z)\| = +\infty\},$$

which is called *basin of attraction of  $\infty$* . It is also easy to see that

$$B_\infty(F_{\mu,\epsilon}) = \bigcup_{n \geq 0} F_{\mu,\epsilon}^{-n}(ext C) \text{ and } B_\infty^c(F_{\mu,\epsilon}) = \bigcap_{n \geq 0} F_{\mu,\epsilon}^{-n}(cl(int C)),$$

where  $\text{int } C$  is the bounded component of the complement of  $C$ ,  $\text{cl}(A)$  and  $A^c$  denote, respectively, the closure and complement of the set  $A$ . Obviously  $B_\infty^c(F_{\mu,\epsilon})$  is the set of points with bounded orbit. The two identities above are satisfied when  $C$  is substituted by any Jordan curve (i.e. a simple and closed curve)  $\Gamma$  such that  $\text{ext } \Gamma \subset B_\infty(F_{\mu,\epsilon})$ ; here  $\text{ext } \Gamma$  has the same meaning of  $\text{ext } C$ .

- The diagonal  $\Delta = \{(x, x) : x \in \mathbb{R}\}$  is always an invariant set for  $F_{\mu,\epsilon}$  and the dynamics on this set is the same of the logistic map  $f_\mu$ . In particular, when  $\mu > 4$  the restriction  $F_{\mu,\epsilon}|_\Delta$  of  $F_{\mu,\epsilon}$  to  $\Delta$  has an invariant Cantor set  $K_\mu$  as its nonwandering set and its dynamics is topologically conjugated to the 2-symbols unilateral shift. On the other hand, when  $\mu > 4$  is large enough, the set of points with bounded orbits  $B_\infty^c(F_{\mu,\epsilon})$  is also a Cantor set, containing properly  $K_\mu$ , and the dynamics of  $F_{\mu,\epsilon}$  on that set is topologically conjugated to the unilateral shift on four symbols.

**2.1. Critical set and image set.** In the study of dynamical systems provided by differentiable and non-invertible transformations the set of critical points and the set of critical values have a relevant role. We recall that for a differentiable endomorphisms the set of critical points is the set of points where the Jacobian matrix is singular. For  $F_{\mu,\epsilon}$  its set of critical points is given by

$$\ell = \ell_1 \cup \ell_2 := \left\{ \left( \frac{1}{2}, y \right) : y \in \mathbb{R} \right\} \cup \left\{ \left( x, \frac{1}{2} \right) : x \in \mathbb{R} \right\};$$

and its set of critical values is  $L := F_{\mu,\epsilon}(\ell) = L_1 \cup L_2$ , where

$$L_1 = F_{\mu,\epsilon}(\ell_1) = \left\{ (x, y) : y = \frac{1-\epsilon}{\epsilon}x - \frac{(1-2\epsilon)\mu}{4\epsilon}, x \leq \frac{\mu}{4} \right\} \text{ and}$$

$$L_2 = F_{\mu,\epsilon}(\ell_2) = \left\{ (x, y) : y = \frac{\epsilon}{1-\epsilon}x + \frac{(1-2\epsilon)\mu}{4(1-\epsilon)}, x \leq \frac{\mu}{4} \right\}.$$

By using these rays is defined the cone

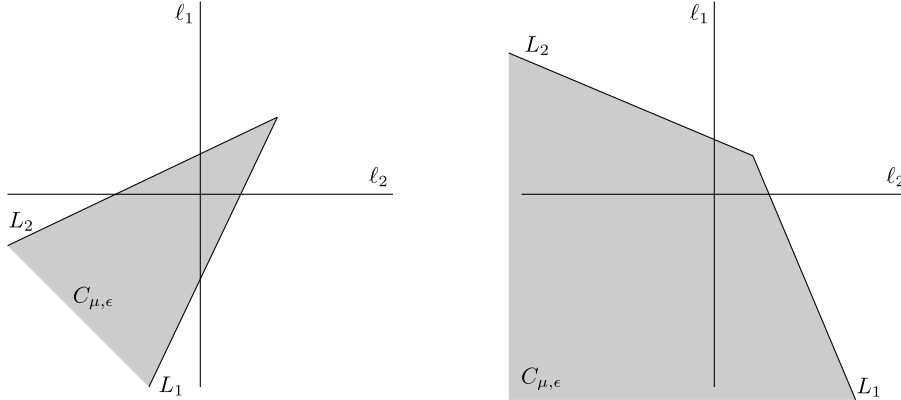


Figure 1: Illustration of the critical set and critical values of  $F_{\mu,\epsilon}$ . Left figure corresponds to small strength, the other one to the large strength; regions in shadow represent  $C_{\mu,\epsilon}$ .

$$C_{\mu,\epsilon} = \left\{ (x, y) : \frac{1-\epsilon}{\epsilon}x - \frac{(1-2\epsilon)\mu}{4\epsilon} \leq y \leq \frac{\epsilon}{1-\epsilon}x + \frac{(1-2\epsilon)\mu}{4(1-\epsilon)}, x \leq \frac{\mu}{4} \right\}.$$

It is easy to check that  $F_{\mu,\epsilon}(\mathbb{R}^2) = C_{\mu,\epsilon}$ ; moreover, every point in the interior of cone  $C_{\mu,\epsilon}$  has four preimages, they are located symmetrically respect to  $\ell_1$  and  $\ell_2$ ; indeed,  $F_{\mu,\epsilon}^{-1}(z, w) = \{(x_{\pm}(z, w), y_{\pm}(z, w))\}$ , where

$$(2.1) \quad \begin{aligned} x_{\pm}(z, w) &= \frac{1}{2} \left[ 1 \pm \sqrt{1 + \frac{4(\epsilon w - (1-\epsilon)z)}{\mu(1-2\epsilon)}} \right] \text{ and} \\ y_{\pm}(z, w) &= \frac{1}{2} \left[ 1 \pm \sqrt{1 + \frac{4(\epsilon z - (1-\epsilon)w)}{\mu(1-2\epsilon)}} \right]; \end{aligned}$$

points outside  $C_{\mu,\epsilon}$  have no preimages, and the restriction of  $F_{\mu,\epsilon}$  to  $\ell_i$  is two-to-one onto  $L_i$ ,  $i = 1, 2$ . In particular, if  $\gamma$  is an injective curve joining  $L_1$  and  $L_2$  with extreme points in these rays and the others ones are in the interior of  $C_{\mu,\epsilon}$ , then  $F_{\mu,\epsilon}^{-1}(\gamma)$  is a Jordan curve symmetric with respect to the critical lines  $\ell_1$  and  $\ell_2$  and surrounding the critical point  $c = (1/2, 1/2)$ .

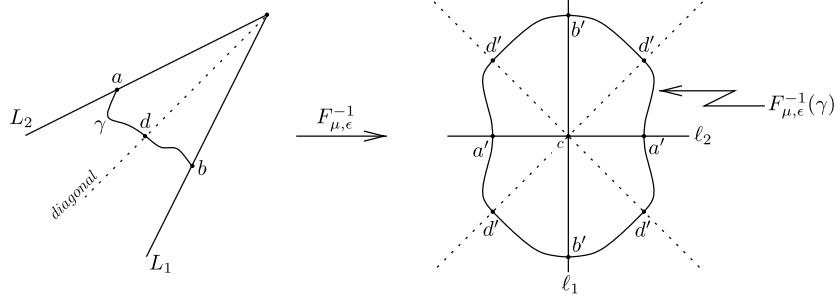


Figure 2: Graphical illustration of how the preimage of a curve  $\gamma$  inside  $C_{\mu,\epsilon}$ , with extremes at  $L_1$  and  $L_2$ , is arranged. The points  $a'$ ,  $b'$  and  $d'$  are, respectively, preimages of  $a$ ,  $b$  and  $d$ .

**2.2. Small strength:  $\epsilon \in (0, 1/2)$ .** In this case there are three curves playing an important meaning in the dynamic description of  $F_{\mu,\epsilon}$ , such a curves are:

$$\epsilon \mapsto \mu_0(\epsilon) = \frac{1}{1-2\epsilon}, \quad \epsilon \mapsto \mu_1(\epsilon) = \frac{4(1-\epsilon)}{1-2\epsilon} \quad \text{and} \quad \epsilon \mapsto \mu'(\epsilon) = 1 + \sqrt{\frac{3-2\epsilon}{1-2\epsilon}};$$

the functions  $\mu_0$  and  $\mu_1$  have the interval  $(0, 1/2)$  as domain, while the domain of  $\mu'$  is  $(0, 3/8]$ . The first curve ( $\epsilon \mapsto \mu_0(\epsilon)$ ) defines the locus where the change in the hyperbolic nature of the fixed point at the origin is marked:  $O$  is a hyperbolic saddle when  $\mu < \mu_0(\epsilon)$  and it is a repeller if  $\mu > \mu_0(\epsilon)$ . At  $\mu = \mu_0(\epsilon)$  the origin has a pitchfork bifurcation and the fixed points  $R(p_{\mu,\epsilon})$  and  $p_{\mu,\epsilon}$  are correctly defined if and only if  $\mu > \mu_0(\epsilon)$ .

From the second curve ( $\epsilon \mapsto \mu_1(\epsilon)$ ) is ensured the existence of a Jordan curve through which is possible to make a description of the basin of attraction of  $\infty$  and its boundary  $\partial B_\infty(F_{\mu,\epsilon})$ . Through this curve is also characterized the location of the intersection point  $(q_{\mu,\epsilon}, 0)$  between  $L_1$  and the horizontal axis, here  $q_{\mu,\epsilon} = \frac{(1-2\epsilon)\mu}{4(1-\epsilon)}$ . Indeed,  $q_{\mu,\epsilon} > 1$  if and only if  $\mu > \mu_1(\epsilon)$ .

The third curve ( $\epsilon \mapsto \mu'(\epsilon)$ ) is related to the *synchronization* of orbits, an important dynamic phenomenon that has captured the attention of several authors.

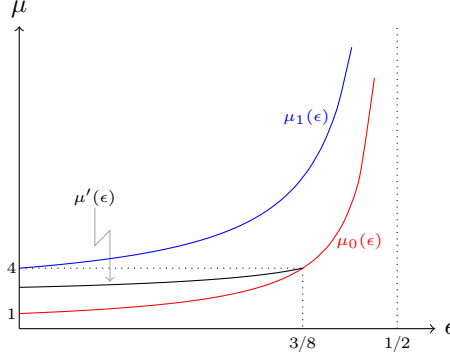


Figure 3: Graphical illustration of the functions  $\epsilon \mapsto \mu_0(\epsilon)$ ,  $\epsilon \mapsto \mu_1(\epsilon)$  and  $\epsilon \mapsto \mu'(\epsilon)$ .

In addition, the first curve is also a reference to the description of the synchronized points. We denote by  $\mathcal{S}(\mu, \epsilon)$  the set of *synchronized points* of  $F_{\mu, \epsilon}$ ; that is, the set of points  $(x, y) \in \mathbb{R}^2$  whose positive orbit is bounded and  $\lim_{n \rightarrow +\infty} |x_n - y_n| = 0$ , where  $(x_n, y_n) = F_{\mu, \epsilon}^n(x, y)$  for all  $n \geq 1$ .

Now we summarize the principal results in [18].

**Theorem A.** *If  $\mu > 1$  and  $\epsilon \in (0, 1/2)$  satisfy  $\mu \leq \mu_1(\epsilon)$ , then there exists a positively invariant Jordan curve  $\Gamma$  containing  $F_{\mu, \epsilon}^{-1}(O)$  such that:*

- a) *The open set  $\text{ext } \Gamma$  is contained in  $B_\infty(F_{\mu, \epsilon})$  and  $\Gamma = \partial B_\infty^o(F_{\mu, \epsilon})$ ; in particular*

$$B_\infty(F_{\mu, \epsilon}) = \bigcup_{n \geq 0} F_{\mu, \epsilon}^{-n}(\text{ext } \Gamma) \quad \text{and} \quad B_\infty^c(F_{\mu, \epsilon}) = \bigcap_{n \geq 0} F_{\mu, \epsilon}^{-n}(\text{cl}(\text{int } \Gamma)).$$

*The symbol  $B_\infty^o(F_{\mu, \epsilon})$  means the unbounded connected component of  $B_\infty(F_{\mu, \epsilon})$  (i.e. the immediate basin of  $\infty$ ) and  $\partial B_\infty^o(F_{\mu, \epsilon})$  denotes its boundary.*

- b) *If  $\mu \leq 4$ , then  $B_\infty(F_{\mu, \epsilon})$  is connected; in this case  $B_\infty(F_{\mu, \epsilon}) = \text{ext } \Gamma$ . On the other hand, when  $4 < \mu \leq \mu_1(\epsilon)$  the basin  $B_\infty(F_{\mu, \epsilon})$  has infinitely many connected components; in this case  $\partial B_\infty(F_{\mu, \epsilon}) = \bigcup_{n \geq 0} F_{\mu, \epsilon}^{-n}(\Gamma)$ .*
- c) *When  $\mu \leq \mu_0(\epsilon)$ ,  $\mathcal{S}(\mu, \epsilon) = B_\infty^c(F_{\mu, \epsilon})$ . Consequently the  $\omega$ -limit set of every point in  $\text{int } \Gamma$  is contained in  $\Delta$ ; further, if  $4 < \mu < \mu_0(\epsilon)$ , then  $\mathcal{S}(\mu, \epsilon)$  is the union of the stable manifolds of the points in the Cantor set on  $\Delta$ . In addition, if  $\mu_0(\epsilon) < \mu \leq \mu'(\epsilon)$ , then  $\mathcal{S}(\mu, \epsilon) = (B_\infty^c(F_{\mu, \epsilon}) \setminus \Gamma) \cup F_{\mu, \epsilon}^{-1}(O)$ .*
- d) *When  $\mu < \mu_0(\epsilon)$ ,  $\Gamma$  is the connected component of the stable manifold  $W^s(O)$  of the origin containing it; moreover,  $W^s(O) = \bigcup_{n \geq 0} F_{\mu, \epsilon}^{-n}(\Gamma)$ . If  $\mu = \mu_0(\epsilon)$ , then  $\Gamma$  contains the unique local center-stable manifold of  $O$ . In particular, for  $\mu \leq \mu_0(\epsilon)$  the curve  $\Gamma$  is  $C^\infty$  and the  $\omega$ -limit set of every  $z \in \Gamma$  is the origin.*

Some comments are natural from the statements in the previous theorem.

**Remark 2.1.** 1) For the parametric region  $\mu_0(\epsilon) < \mu \leq \mu_1(\epsilon)$ , the curve  $\Gamma$  is obtained as a collage of four others, one of them, denoted by  $\Gamma_b$ , has extreme points at  $O$  and  $S = (1, 0)$ , it is the graph of some function  $\gamma : [0, 1] \rightarrow \mathbb{R}$  which

is contained in  $D = cl(int C) \cap \{(x, y) : y \leq 0\}$ . Indeed,  $\gamma$  is the fixed point of a contracting operator acting on the complete metric space of functions defined in  $[0, 1]$  such that each one of them has Lipschitz constant less or equal than 1, it is symmetric respect to  $1/2$ , fixes  $t_0 = 0$ , its graph is in  $D$  and it is tangent to the antidiagonal at  $t_0$ . The distance in this space is the usual between bounded functions. Thus, the curve  $\Gamma$  is given by  $\Gamma = \Gamma_b \cup \Gamma_t \cup \Gamma_\ell \cup \Gamma_r$  where

$$(2.2) \quad \begin{aligned} \Gamma_t &= \{(t, 1 - \gamma(t)) : t \in [0, 1]\}, \Gamma_\ell = \{(\gamma(t), t) : t \in [0, 1]\} \\ \text{and } \Gamma_r &= \{(1 - \gamma(t), t) : t \in [0, 1]\}; \end{aligned}$$

in addition,  $F_{\mu, \epsilon}^{-1}(\Gamma_b) = \Gamma_b \cup \Gamma_t$ ,  $F_{\mu, \epsilon}^{-1}(\Gamma_\ell) = \Gamma_\ell \cup \Gamma_r$  and  $F_{\mu, \epsilon}(\Gamma) \subset \Gamma_b \cup \Gamma_\ell$ ; see Figure 4. That operator is defined as follows: given a function in that space, the

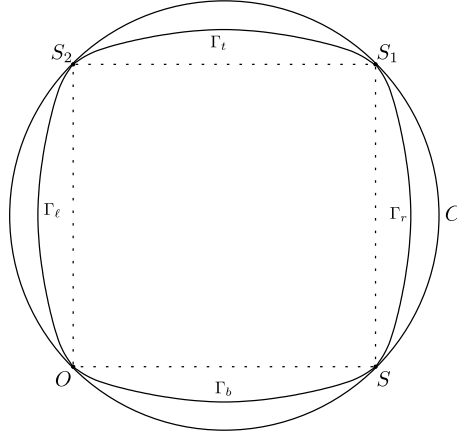


Figure 4: Idealization of the Jordan curve  $\Gamma = \Gamma_b \cup \Gamma_t \cup \Gamma_\ell \cup \Gamma_r$ , which is also obtained as the limit curves given by the preimages of the circle  $C$ .

preimage under  $F_{\mu, \epsilon}$  of its graph is union of two graphs: one of them is located above  $\ell_2$ , it joins the  $S_1 = (1, 1)$  and  $S_2 = (0, 1)$ ; the other one is below  $\ell_2$  and connects the points  $O$  with  $S$ . Just the function defining this last graph is the image of the operator of the given function.

If  $\mu$  and  $\epsilon$  satisfy  $1 < \mu \leq \mu_0(\epsilon)$ , the operator above is not necessarily a contraction. However, to obtain  $\Gamma$  one takes the curve given by the arc of the circle  $C$  in  $D$ , then the forward iterations of this arc under the operator above define an increasing sequence of functions whose limit function and the preceding collage determine a positively invariant Jordan curve whose unbounded component of its complement is contained in  $B_\infty(F_{\mu, \epsilon})$ ; the uniqueness of such a curve is consequence of the synchronization property due to the coincidence of  $\Gamma$  with the stable ( $1 < \mu < \mu_0(\epsilon)$ ) and center-stable ( $\mu = \mu_0(\epsilon)$ ) manifold of the origin. In this way, for all  $\mu$  and  $\epsilon$  with  $1 < \mu \leq \mu_1(\epsilon)$ , the curve  $\Gamma$  is the unique positively invariant Jordan curve such that  $F_{\mu, \epsilon}^{-1}(O) \subset \Gamma$  and  $ext \Gamma = B_\infty^o(F_{\mu, \epsilon})$ .

2) For all  $\mu$  and  $\epsilon \in (0, 1/2)$  with  $4 < \mu \leq \mu_1(\epsilon)$  the attraction basin  $B_\infty(F_{\mu, \epsilon})$  has infinitely many connected components inside  $int \Gamma$ . For this sector in the parameter

space it is proved that there are two points  $p_i \in L_i \cap \Gamma$  ( $i = 1, 2$ ) such that the arc of  $\Gamma$  containing  $p_1, p_2$  and  $S_1$  and the pieces of those rays between  $p_1, p_2$  and  $d_\mu = (\mu/4, \mu/4)$  determine a triangular region in  $ext \Gamma$  in such a way that its preimage under  $F_{\mu, \epsilon}$  defines a connected component of  $B_\infty(F_{\mu, \epsilon})$  inside  $int \Gamma$  whose boundary is part of  $F_{\mu, \epsilon}^{-1}(\Gamma)$  and surrounds the critical point  $c$ ; see Figure 5. Just the recursive

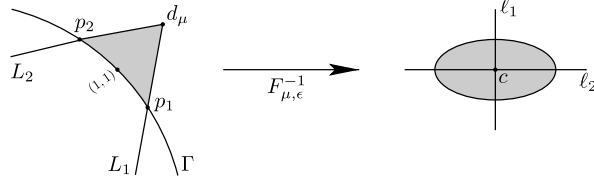


Figure 5: The connect component of  $B_\infty(F_{\mu, \epsilon})$  inside  $int \Gamma$  (shaded region on the right side) is obtained as preimage of the triangular region described above.

preimages of this component produce infinitely many other connected components of  $B_\infty(F_{\mu, \epsilon})$  inside  $int \Gamma$ . Every component in the segment  $OS_1$  of the complement of the Cantor set  $K_\mu$  is contained in some of those preimages and each of which contains at most two components of  $K_\mu^c$  in that segment.

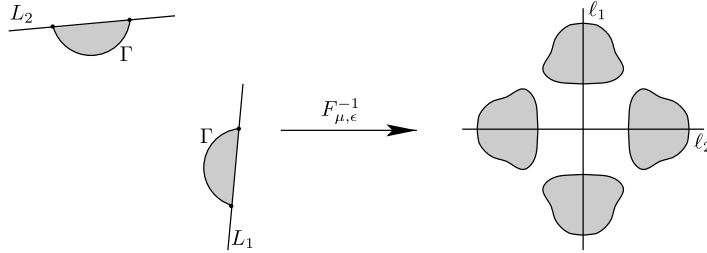


Figure 6: In the left side it is illustrates a pair of sectors (shaded regions) whose preimages, except their boundaries, are components of  $B_\infty(F_{\mu, \epsilon})$  inside  $int \Gamma$ ; observe that they do not intersect the segment  $OS_1$ .

It is also possible that there are other components of  $B_\infty(F_{\mu, \epsilon})$  inside  $int \Gamma$  such that none of its images or preimages intersects the complement of  $K_\mu$  in  $\Delta$ . These other components of  $B_\infty(F_{\mu, \epsilon})$  are produced only as preimages of sectors bounded by an arc in  $\Gamma$  and a segment in  $L_1$  (resp.  $L_2$ ) with the same extreme points, such that each one of these sectors, except that arc, is contained in  $ext \Gamma$ . In view of the nice symmetric properties of  $\Gamma$  respect to  $l_1$  and  $l_2$ , this kind of sectors appear in pairs, one is the reflection of the other. The preimage of each one of these sectors is the disjoint union of two topological disks displayed symmetrically and whose boundaries are contained in  $F_{\mu, \epsilon}^{-1}(\Gamma)$ ; see Figure 6.

Now consider  $\mu > 1$  and  $\epsilon \in (0, 1/2)$  such that  $\mu > \mu_1(\epsilon)$ , that is  $q_{\mu, \epsilon} > 1$ ; recall the meaning of the curve  $\epsilon \mapsto \mu_1(\epsilon)$  above. In this case two mutually exclusive situations occur: either there exists an integer  $n \geq 0$  such that  $F_{\mu, \epsilon}^{-n}(C)$

is contained into the interior of  $C_{\mu,\epsilon}$ , or for all  $n \geq 0$  the connect component of  $F_{\mu,\epsilon}^{-n}(C)$  containing  $O$  also contains  $F_{\mu,\epsilon}^{-1}(O)$  and intersect the rays  $L_1$  and  $L_2$ . In the first configuration the set of points with bounded orbit has infinitely components and none of them contains  $F_{\mu,\epsilon}^{-1}(O)$ , hence it is impossible the existence of a Jordan as above; observe that if  $\mu$  is large enough, then this arrangement is achieved. In the second situation, we do not know a theoretical result guaranteeing the existence of such a curve; however, when  $\mu$  is close enough to  $\mu_1(\epsilon)$  there are computacional simulations that suggest such an existence; see Figure 27. Observe that for any curve in  $D$  joining  $O$  and  $S$  its preimage under  $F_{\mu,\epsilon}$  is disjoint union of four arcs: two above  $\ell_2$  and two below it; each one of these arcs connects a preimage of  $O$  with the closest preimage of  $S$ ; see Figure 7. Despite this difficulty one can define

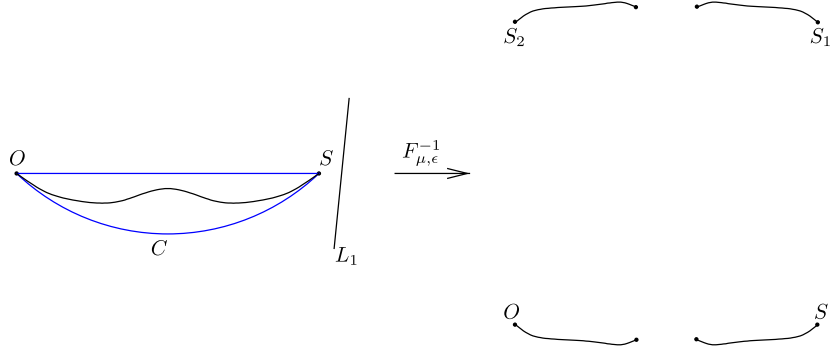


Figure 7: In the right side of the figure is illustrated the preimage of the curve contained in  $D$  (left side) when  $\mu > \mu_1(\epsilon)$ , i.e. when  $q_{\mu,\epsilon} > 1$ .

a similar operator to the previous and then try to get, in some sense, a limit curve for the iterations of that operator. The ideas of such a procedure are the same as those discussed in item 3 of Remark 2.2. This is still under development, we hope to present results in a forthcoming article.

**2.3. Large strength:  $\epsilon < 0$ .** When the parameters  $\mu$  and  $\epsilon$  are such that  $\mu > 1$  and  $\epsilon < 0$  (or equivalently  $\epsilon > 1$ ) the fixed points of  $F_{\mu,\epsilon}$  have different nature than in the small strength case. In particular, for the fixed points on the diagonal,  $O$  and  $P_\mu$ , are well known the following facts:

- (i) The origin  $O$  is always a hyperbolic repeller.
- (ii) If  $1 < \mu < \mu'_0(\epsilon) := \frac{1-4\epsilon}{1-2\epsilon}$ , then  $P_\mu$  is a hyperbolic saddle.
- (iii) When  $\mu'_0(\epsilon) < \mu < \mu_2(\epsilon) := \frac{3-4\epsilon}{1-2\epsilon}$ ,  $P_\mu$  is a hyperbolic attractor.
- (iv) If  $\mu_2(\epsilon) < \mu < 3$ , then  $P_\mu$  is again a hyperbolic saddle.
- (v) For  $\mu > 3$ ,  $P_\mu$  is always a hyperbolic repeller.

The fixed points outside the diagonal,  $p_{\mu,\epsilon}$  and  $R(p_{\mu,\epsilon})$ , appear when  $\mu > \mu'_0(\epsilon)$ . The curve  $\{(\epsilon, \mu'_0(\epsilon)) : \epsilon < 0\}$  is the locus where a pitchfork bifurcation occurs for the fixed point  $P_\mu$ . Another curve in the parameter space with a prominent



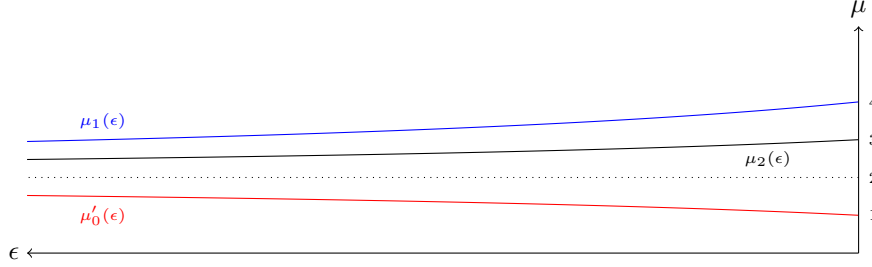


Figure 8: Graphs of the functions  $\epsilon \mapsto \mu'_0(\epsilon)$ ,  $\epsilon \mapsto \mu_1(\epsilon)$  and  $\epsilon \mapsto \mu_2(\epsilon)$ .

performance is given by  $\mu_1(\epsilon) := \frac{4(1-\epsilon)}{1-2\epsilon}$ . As in the case of small strength, the curve  $\{(\epsilon, \mu_1(\epsilon)) : \epsilon < 0\}$  determines the region in the parameter space where:

- The intersection point  $(q_{\mu,\epsilon}, 0)$  between  $L_1$  and the  $x$ -axis is outside the square  $Q = [0, 1] \times [0, 1]$ ; indeed,  $q_{\mu,\epsilon} \leq 1$  if, and only if,  $\mu \leq \mu_1(\epsilon)$ .
- It is guaranteed the existence of an invariant curve providing information about  $B_\infty(F_{\mu,\epsilon})$  and its boundary, see statement below.

The square  $Q$  refines the first estimate of the basin of attraction of  $\infty$ : the boundary  $\partial Q$  of  $Q$  is such that  $\text{ext } \partial Q$  is contained in  $B_\infty(F_{\mu,\epsilon})$ , hence

$$B_\infty(F_{\mu,\epsilon}) = \bigcup_{n \geq 0} F_{\mu,\epsilon}^{-n}(\text{ext } \partial Q) \quad \text{and} \quad B_\infty^c(F_{\mu,\epsilon}) = \bigcap_{n \geq 0} F_{\mu,\epsilon}^{-n}(Q);$$

in addition,  $\partial Q \setminus F_{\mu,\epsilon}^{-1}(O) \subset B_\infty(F_{\mu,\epsilon})$ .

Now we compile the statements of the more relevant results in [17].

**Theorem B.** *If  $\mu > 1$  and  $\epsilon < 0$  satisfy  $\mu \leq \mu_1(\epsilon)$ , then there exists a Lipschitzian and positively invariant curve  $\Gamma$  containing  $F_{\mu,\epsilon}^{-1}(O)$  and the fixed points outside the diagonal, such that:*

- If  $\mu'_0(\epsilon) < \mu \leq \mu_1(\epsilon)$ , then  $\Gamma$  is a Jordan curve and  $\text{ext } \Gamma = B_\infty^o(F_{\mu,\epsilon})$ ; in other words,  $\text{ext } \Gamma \subset B_\infty(F_{\mu,\epsilon})$  and  $\Gamma = \partial B_\infty^o(F_{\mu,\epsilon})$ . As in the small strength case

$$B_\infty(F_{\mu,\epsilon}) = \bigcup_{n \geq 0} F_{\mu,\epsilon}^{-n}(\text{ext } \Gamma) \quad \text{and} \quad B_\infty^c(F_{\mu,\epsilon}) = \bigcap_{n \geq 0} F_{\mu,\epsilon}^{-n}(\text{cl}(\text{int } \Gamma)).$$

- When  $\mu \leq \mu'_0(\epsilon)$  the curve  $\Gamma$  is the union of the straight segments  $OS_1$  and  $SS_2$ . In this case,  $B_\infty(F_{\mu,\epsilon}) = \mathbb{R}^2 \setminus \Gamma$  and the  $\omega$ -limit set of every point  $z$  in  $\Gamma \setminus F_{\mu,\epsilon}^{-1}(O)$  is  $P_\mu$ ; that is  $F_{\mu,\epsilon}^n(z) \rightarrow P_\mu$  if  $n \rightarrow +\infty$ .

**Remark 2.2.** 1) Let  $T$  be the closed triangular region defined by the vertices  $O, S$  and  $c = (1/2, 1/2)$ . Denote by  $Lip_1$  the complete metric space of all the Lipschitzian functions  $h : [0, 1] \rightarrow \mathbb{R}$  with Lipschitz constant  $L(h) \leq 1$  such that:  $h(t) = h(1-t)$  for all  $t \in [0, 1/2]$ ,  $h(0) = 0$  and whose graph is contained in  $T$ ; the distance here the usual one between bounded functions. Given any  $h \in Lip_1$ , its graph intersects  $L_1$  in only one point  $(t^*, h(t^*))$  where  $0 < t^* \leq 1$ ; so, by using (2.1)

$$\{(x_-(t, h(t)), y_-(t, h(t))) : t \in [0, t^*]\} \cup \{(x_+(t, h(t)), y_-(t, h(t))) : t \in [0, t^*]\}$$

is a graph of some function in  $Lip_1$ . This fact describes an assignment defining an operator  $\Psi$  on  $Lip_1$ , which is not necessarily a contraction; so to obtain  $\Gamma$  one begins with the null function  $h_0$  and consider its forward orbit  $(h_n)_{n \geq 0}$ , with  $h_n = \Psi^n(h_0)$ . Then it is proved that  $h_n(t) < h_{n+1}(t)$  for all  $n \geq 0$  and  $t \in (0, 1)$ . Hence a limit function  $\hat{h} \in Lip_1$  is obtained, which is clearly a fixed point of  $\Psi$ . Through the expanding property of the origin it is showed that the graph of  $\hat{h}$ , in what follows  $\Gamma_b$ , is tangent to the diagonal and the antidiagonal at  $O$  and  $S$ , respectively; with this graph is constructed the juxtaposition  $\Gamma = \Gamma_b \cup \Gamma_t \cup \Gamma_\ell \cup \Gamma_r$ , where  $\Gamma_t, \Gamma_\ell$  and  $\Gamma_r$  are as in the small strength case. At this point, if  $\mu'_0(\epsilon) < \mu \leq \mu_1(\epsilon)$ , then is proved that  $\hat{h}(t) < t$  for all  $t \in (0, 1/2]$  and the fixed points  $p_{\mu, \epsilon}$  and  $R(p_{\mu, \epsilon})$  are in  $\Gamma$ ; moreover,  $\Gamma \setminus F_{\mu, \epsilon}^{-1}(O) \subset \text{int } Q$  and  $\Gamma$  is a Jordan curve with  $\text{ext } \Gamma \subset B_\infty(F_{\mu, \epsilon})$ . On the other hand, when  $1 < \mu \leq \mu'_0(\epsilon)$  it is used the hyperbolic nature of the fixed point  $P_\mu$  to show that  $\Gamma_b = \{(t, t) : t \in [0, 1/2]\} \cup \{(t, 1-t) : t \in [1/2, 1]\}$  and  $B_\infty(F_{\mu, \epsilon}) = \mathbb{R}^2 \setminus \Gamma$ .

We complement these facts with the following:

**Problem.** For all  $\mu > 1$  and  $\epsilon < 0$  with  $\mu'_0(\epsilon) \leq \mu \leq \mu_2(\epsilon)$  the set of synchronized points  $\mathcal{S}(\mu, \epsilon)$  agrees with  $\text{int } \Gamma \cup F_{\mu, \epsilon}^{-1}(O)$ ; moreover,  $\lim_{n \rightarrow +\infty} F_{\mu, \epsilon}^n(z) = P_\mu$  for every point  $z$  in  $\text{int } \Gamma$ ,  $B_\infty^c(F_{\mu, \epsilon}) = \text{cl}(\text{int } \Gamma)$  and  $\lim_{n \rightarrow +\infty} F_{\mu, \epsilon}^n(z)$  is either  $p_{\mu, \epsilon}$  or  $R(p_{\mu, \epsilon})$  whenever  $z \in \Gamma \setminus F_{\mu, \epsilon}^{-1}(O)$ .

As in the small strength case, we think that the region in the parameter space where  $\mathcal{S}(\mu, \epsilon) = (B_\infty^c(F_{\mu, \epsilon}) \setminus \Gamma) \cup F_{\mu, \epsilon}^{-1}(O)$  can also be increased.

2) In relation with the existence of components of  $B_\infty(F_{\mu, \epsilon})$  inside  $\text{int } \Gamma$  there is a noticeable difference with the small strength case. When  $\mu \leq \mu_1(\epsilon)$ , so  $\mu \leq 4$ , it is possible that  $B_\infty(F_{\mu, \epsilon}) \cap \text{int } \Gamma \neq \emptyset$ ; indeed, this happens if and only if the curve  $\Gamma_r$  (resp.  $\Gamma_t$ ) passes across  $L_1$  (resp.  $L_2$ ). In this case every component of  $B_\infty(F_{\mu, \epsilon})$  inside  $\text{int } \Gamma$  is a preimage of one of the regions determined by either  $\Gamma_r$  and  $L_1$  or  $\Gamma_\ell$  and  $L_2$ , as explained in item 2 of Remark 2.1; see Figure 6. In figures 28 (picture in the right side) and 29 we show a numerical evidence of this fact. On the other hand, when  $\mu > 4$  it follows that  $q_{\mu, \epsilon} > 1$  and so the square  $Q$  is in the topological interior of the cone  $C_{\mu, \epsilon}$ , this implies that there is no an invariante curve contained in  $Q$  and containing  $F_{\mu, \epsilon}^{-1}(O)$ ; indeed,  $B_\infty^c(F_{\mu, \epsilon})$  has infinitely many components. In fact,  $F_{\mu, \epsilon}^{-1}(Q)$  is disjoint union of four compact sets:  $Q_0, Q_1, Q_2$  and  $Q_3$ ; thus, for all  $n \geq 1$  it holds that  $F_{\mu, \epsilon}^{-n}(Q)$  is union of  $4^n$  compact sets  $Q_{i_0 \dots i_{n-1}}$  with  $i_0, \dots, i_{n-1} \in \{0, 1, 2, 3\}$  such that:  $Q_{i_0 \dots i_n} \subset Q_{i_0 \dots i_{n-1}}$ ,  $F_{\mu, \epsilon}(Q_{i_0 \dots i_n}) = Q_{i_1 \dots i_n}$  and  $z \in Q_{i_0 \dots i_n}$  if and only if  $F_{\mu, \epsilon}^j(z) \in Q_{i_j}$  for every  $0 \leq j \leq n$ . Therefore,  $B_\infty^c(F_{\mu, \epsilon})$  is the union of the nested intersections  $\bigcap_{n \geq 0} Q_{i_0 \dots i_n}$ , where  $i_n \in \{0, 1, 2, 3\}$  for all  $n \geq 0$ . Moreover, if  $\mu > 4$  is large enough, then  $B_\infty^c(F_{\mu, \epsilon})$  is a Cantor set.

3) When  $\mu > 1$  and  $\epsilon < 0$  satisfy  $\mu_1(\epsilon) < \mu < 4$  there is still the possibility of having a positively invariant curve through the points in  $F_{\mu, \epsilon}^{-1}(O)$ . In what follows we will describe a procedure by which we believe that such a curve  $\Gamma$  is obtained as limit of a sequence of curves  $(\Gamma_n)_{n \geq 1}$  containing  $F_{\mu, \epsilon}^{-1}(O)$ . Take  $\mu$  and  $\epsilon$  as above, so  $L_1$  (resp.  $L_2$ ) meets  $\partial Q$  in a point  $q$  (resp.  $R(q)$ ) on the segment  $SS_1$  (resp.  $S_1S_2$ ). The preimage under  $F_{\mu, \epsilon}$  of the segments  $OS$  and  $Sq$  gives two curves:  $\Gamma_1^b$  and  $\Gamma_1^t$ ,

the first one connects  $O$  and  $S$ , the other one joins  $S_1$  and  $S_2$ . In the same way, the preimage of the segments  $OS_2$  and  $S_2R(q)$  is union of the curves:  $\Gamma_1^\ell = R(\Gamma_1^b)$  and  $\Gamma_1^r = R(\Gamma_1^t)$ ; recall that  $R(x, y) = (y, x)$  for all  $(x, y) \in \mathbb{R}^2$ . Hence a closed curve containing  $F_{\mu, \epsilon}^{-1}(O)$  is obtained:  $\Gamma_1 = \Gamma_1^b \cup \Gamma_1^t \cup \Gamma_1^\ell \cup \Gamma_1^r$ . To continue with the construction of the sequence above it is introduced the linear order  $<$  on  $\Gamma_1^r$ :

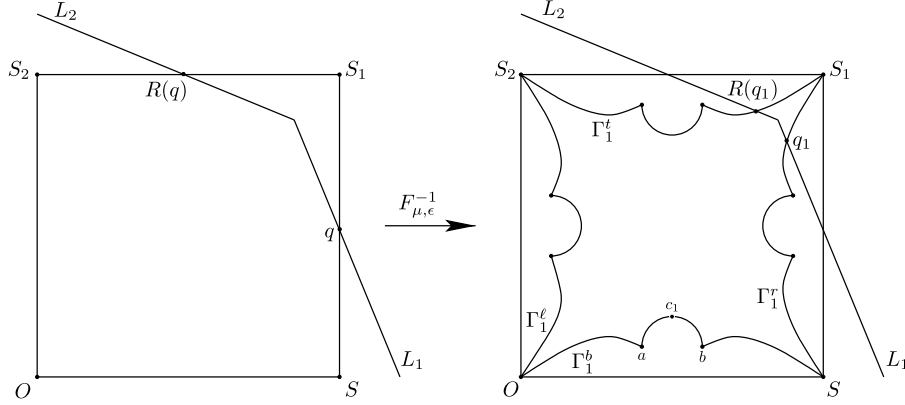


Figure 9: First step in the construction of the sequence  $(\Gamma_n)_{n \geq 1}$  which leads to a positively invariant curve through points in  $F_{\mu, \epsilon}^{-1}(O)$ .

given  $z, w \in \Gamma_1^r$ , it is said that  $z < w$  if and only if in the route along  $\Gamma_1^r$ , from  $S$  to  $S_1$ ,  $z$  is first than  $w$ . In this order, let  $q_1$  be the first point on  $\Gamma_1^r$  meeting  $L_1$ ; clearly  $R(q_1)$  is the analagous point on  $\Gamma_1^t$  from  $S_2$  to  $S_1$ , see Figure 9. The curve  $\Gamma_2$  is obtained taking the preimage of the arcs  $\widehat{OSq_1}$  and  $\widehat{OS_2R(q_1)}$  on  $\Gamma_1$ . Next, repeat the same procedure, including the order above, to construct the remaining curves  $\Gamma_n$ . It should be highlighted that for each  $n \geq 1$  the curve  $\Gamma_n^b$  contains the points  $a$  and  $b$  of  $F_{\mu, \epsilon}^{-1}(S)$  that are located below  $\ell_2$ ; in addition, if  $c_n$  is the point of  $F_{\mu, \epsilon}^{-1}(q_{n-1})$  ( $q_0 = q$ ) in  $\Gamma_n^b$ , then the arc  $\widehat{ac_nb}$  is the part of the preimage of the piece on  $\Gamma_{n-1}^r$  from  $S$  to  $q_{n-1}$  ( $\Gamma_0^r$  is the segment  $SS_1$  on  $\partial Q$ ); that arc is a kind of bubble that connects the two arcs in  $\Gamma_n^b$  produced by means of the preimage of  $\Gamma_{n-1}^b$ ; see Figure 9 for the case  $n = 1$ .

A couple of important remarks about the sequence  $(\Gamma_n)_{n \geq 1}$  and its limit curve  $\Gamma$  are necessary. First, for  $n$  large enough the curve  $\Gamma_n^b$ , even  $\Gamma^b$ , may not be the graph of a function; this loss is essentially due to the fact that the origin is a hyperbolic repeller and the expansion on the antidiagonal is greater than the expansion on the diagonal, which implies that the slope of  $\Gamma_n^b$  at  $S$  is asymptotic to  $-1$ . Thus,  $\Gamma_n^b$  and  $\Gamma_n^r$  look tangent to the antidiagonal at  $S$  when  $n$  is large enough. This configuration is propagated by preimages, so in a neighborhood of the point  $a$ , and also at  $b$ , the vertical line test indicates that  $\Gamma_n^b$  is not the graph of a function when  $n$  is large enough. Figure 10 illustrates how the curve  $\Gamma_n^b$  loses the graph nature when  $n$  is large enough, see also Figure 31. The second remark is related to the possibility that  $\text{ext } \Gamma \cap B_\infty^c(F_{\mu, \epsilon}) \neq \emptyset$ . To be able to argue this possible phenomenon, suppose

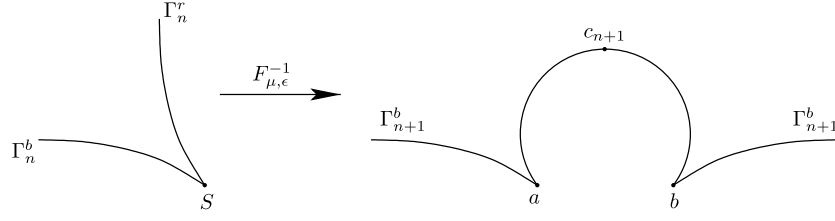


Figure 10: Asymptotic tangency of curves  $\Gamma_n^b$  and  $\Gamma_n^r$  at  $S$  implies the breaking of the graph condition for the curve  $\Gamma_{n+1}^b$  near the points  $a$  and  $b$ .

that for some  $n \geq 1$  there are points  $r_1, r_2 \in \Gamma_n^r$  such that, in the order considered in  $\Gamma_n^r$ , it holds that  $q_n < r_1 < r_2$  and the arc in  $\Gamma_n^r$  containing  $r_1$  and  $r_2$  is contained in the cone  $C_{\mu, \epsilon}$ ; so, the preimage of this arc (which is not considered to obtain  $\Gamma_{n+1}$ ) is union of two closed curves contained in  $\text{ext } \Gamma_{n+1}$ ; see Figure 11 where this possibility is grossly illustrated. Observe that if this arrangement is also on

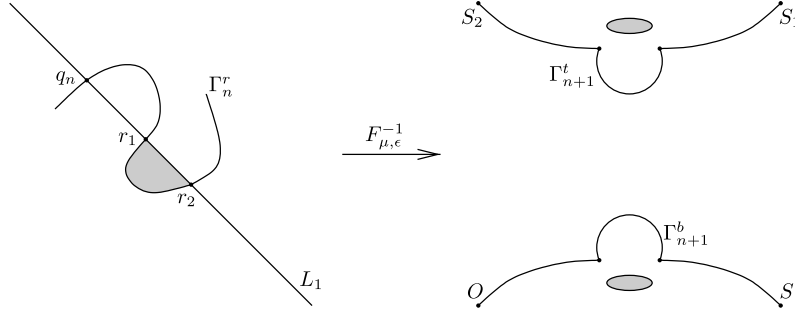


Figure 11: An outline of the configuration on  $\Gamma_n$  that provides bounded orbits in  $\text{ext } \Gamma_{n+1}$ .

the limit curve  $\Gamma$ , then the preimage of an arc as described for  $\Gamma_n^r$  but now on  $\Gamma^r$  produces components of  $B_\infty(F_{\mu, \epsilon})$  in  $\text{ext } \Gamma$  whose boundaries are points with omega limit set contained in  $\Gamma$ .

### 3. NUMERICAL EVIDENCES

In this section we will report part of the results of computational simulations that we have done to try to understand a little more the complicated dynamics of  $F_{\mu, \epsilon}$ . Indeed, we display some figures generated by forward or backward iterations of certain points in order to try to obtain information about  $B_\infty(F_{\mu, \epsilon})$ , its boundary and even other dynamic behaviors that are not theoretically described. Figures shown below were generated using Fractint, a freeware fractal generator (<https://www.fractint.org/>). By means of this platform we illustrate several results discussed in [17] and [18], and some other possible dynamic phenomena that by the complicated nature and the absence of appropriate theoretical tools, they have not been addressed with adequate mathematical rigor. Indeed, we hope that

based on these computational simulations one can follow the heuristic principle for further analytical examination that allows to explain phenomena such as Hopf bifurcations or existence of fat attractors, which, due to the numerical evidences, could be displayed in the dynamic of the coupled logistic map (1.1).

In this computational platform we introduce a program to plot forward and backward iterations of points under  $F_{\mu,\epsilon}$ , it is also plotted preimages of the circle  $C$  and the boundary of the square  $Q$ . Some comments are necessary before showing a collection of figures produced with Fractint. When the backward iteration of a point is done, the points plotted outline a figure in which two zones appear: a dark one (preimages of the point) containing part of the complement of  $B_\infty(F_{\mu,\epsilon})$  and a white zone that does not show preimages of the point by one of the following reasons: either the number of iterated is insufficient or such white zones are part of the basin of attractors, one of them the attractor at  $\infty$  and possibly other attractors contained in the bounded component of the boundary of the immediate basin of  $\infty$ .

Our program is concentrated in five subroutines:

**Option 0.** Given an integer  $n \geq 0$  and  $(x, y) \in \mathbb{R}^2$ , every point  $F_{\mu,\epsilon}^k(x, y)$  with  $0 \leq k \leq n$  is plotted. With this option possible attractors should be detected.

**Option 1.** For  $n \geq 0$  and  $(x, y) \in \mathbb{R}^2$  all the possible points in  $F_{\mu,\epsilon}^{-n}(x, y)$  are plotted; recall that  $(x, y)$  has preimage if and only if  $(x, y) \in C_{\mu,\epsilon}$ . This tool allows to get an idea of the invariant curve  $\Gamma$  in theorems A, B and remarks 2.1, 2.2.

**Option 2.** This option is a combination of the previous ones. Given a point  $(x, y)$  and nonnegative integers  $n_1, n_2$  with  $n_1 + n_2 > 0$ , for each  $0 \leq j \leq n_1$  Option 1 is applied to  $F_{\mu,\epsilon}^j(z)$  with  $n = n_2$ .

**Option 3.** It is a subroutine to plot preimages of the circle  $C$ ; it is a tool to visualize approximations of the curve  $\Gamma$  in the small strength case.

**Option 4.** This is similar to Option 3 but  $C$  is replaced by the boundary of square  $Q$ . It is useful to have information about  $\Gamma$  in the large strength case.

In each of the figures shown in paragraphs 3.1 and 3.2 are notified the values of  $\mu$  and  $\epsilon$ , in some cases option used is also informed.

**3.1. Small strength case.** Here we discuss some scenarios of how the curve  $\Gamma$  and its preimages are arranged. With the help of computational simulations we also show a collections of figures evidencing several kind of attracting sets, some of which are related with possible Hopf bifurcations.

**3.1.1. On the synchronization case.** Consider the region in the parameter space where it has been proved that synchronization occurs (see item c of Theorem A), that is  $1 < \mu \leq \max\{\mu'(\epsilon), \mu_0(\epsilon)\}$ . For all  $\mu$  and  $\epsilon$  in this sector it is clear that  $B_\infty(F_{\mu,\epsilon}) = ext\Gamma$  and  $\partial B_\infty(F_{\mu,\epsilon}) = \Gamma$ ; in addition, every point inside  $int\Gamma$  has its omega limit set contained in the segment  $OS_1$ . However the fashion in which preimages of  $\Gamma$  are arranged is not uniform in that parameter region. In fact, if  $\mu < 4$ , then  $\Gamma$  is completely invariant:  $F_{\mu,\epsilon}^{-1}(\Gamma) = \Gamma$ ; the picture in the left side in Figure 12 shows the manner in which  $\Gamma$  and its preimage appear in this case. When  $\mu = 4$ , the countable set  $\bigcup_{n \geq 0} F_{\mu,\epsilon}^{-n}(\Gamma)$  has a non-trivial part inside

$int \Gamma$ ; in fact, the set of points  $q$  in the segment  $OS_1$  such that  $F_{\mu,\epsilon}^n(q) = S_1$  for some  $n \geq 0$  is dense in that segment. Now, when  $\mu > 4$  every component of the preimages of  $\Gamma$  is a continuum (compact and connected) set. In what follows we discuss about this fact; before a possible configuration of  $\bigcup_{n \geq 0} F_{\mu,\epsilon}^{-n}(\Gamma)$  is shown in right picture of Figure 12. Recall that if  $\mu > 4$ , then  $B_\infty(F_{\mu,\epsilon})$  has infinitely many

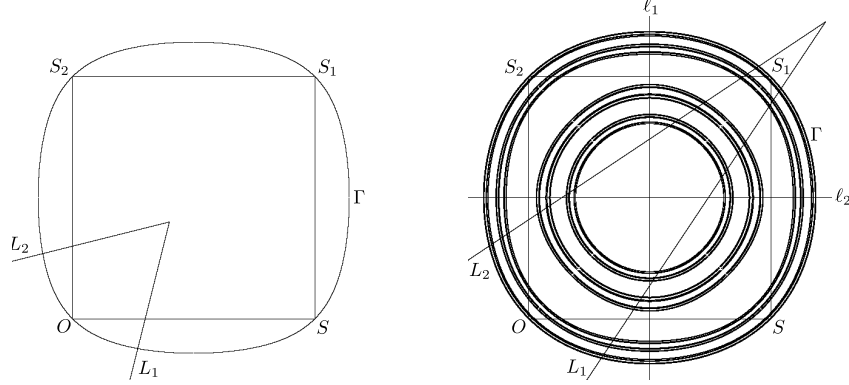


Figure 12: In these pictures are shown large backward iterations of the circle  $C$ . In the left one  $\mu = 1.6$  and  $\epsilon = 0.2$ , for the picture on the right side  $\mu = 4.9$  and  $\epsilon = 0.4$ . The indicated curve  $\Gamma$  is actually an approximation to the Jordan curve in Theorem A; that approximation in the right side is just the external border of that picture.

components in  $int \Gamma$ ; see first part of item 2 in Remark 2.1. These components are arranged generically in two special ways; to explain them consider the set  $P(O)$  of all the preimages of  $O$  on the diagonal, also consider the Cantor set  $K_\mu$  defined dynamically by the logistic map  $f_\mu$ ; clearly  $P(O)$  is a proper subset of  $K_\mu$ . Let  $T$  be the triangular region introduced at the beginning of item 2 in Remark 2.1. So,  $F_{\mu,\epsilon}^{-1}(T)$  is a topological disk whose interior is contained in  $B_\infty(F_{\mu,\epsilon})$  and its boundary is the Jordan curve obtained as preimage of the arc  $\widehat{p_1 p_2}$  on  $\Gamma$  as defined in Remark 2.1, see Figure 5. Recall that for a simple curve inside  $C_{\mu,\epsilon}$  with extreme points at  $L_1$  and  $L_2$ , its preimage is always a topological circle (a circle, for short) surrounding  $c = (1/2, 1/2)$ ; this preimage is generically either in the interior of  $C_{\mu,\epsilon}$  or its intersection with that cone is union of two disjoint curves with extreme points at  $L_1$  and  $L_2$ . From now on we say that a curve *goes through*  $L_1$  and  $L_2$  if it is contained inside  $C_{\mu,\epsilon}$  with extreme points in  $L_1$  and  $L_2$ .

**First way:** *The boundary of  $F_{\mu,\epsilon}^{-1}(T)$  goes through  $L_1$  and  $L_2$ .*

In this instance, the preimage of  $F_{\mu,\epsilon}^{-1}(T)$  is a closed topological annulus (an annulus, for short) such that: its interior is part of  $B_\infty(F_{\mu,\epsilon})$  and each circle of its boundary cuts  $P(O) \setminus \{O, S_1\}$  in two points and goes through  $L_1$  and  $L_2$ . Repeating this argument recursively one can describe the components of  $B_\infty(F_{\mu,\epsilon})$  inside  $int \Gamma$ . The following facts are clear:

- (a) For every  $n \geq 2$ ,  $F_{\mu,\epsilon}^{-n}(T)$  is disjoint union of  $2^{n-2}$  annuli whose interiors is in  $B_\infty(F_{\mu,\epsilon})$ ; as above, each circle in the boundary of every annulus in  $F_{\mu,\epsilon}^{-n}(T)$  goes through  $L_1$  and  $L_2$ , and also cuts  $P(O) \setminus \{O, S_1\}$  exactly in two points.
- (b)  $P(O) = \{O, S_1\} \cup \bigcup_{n \geq 1} (\partial F_{\mu,\epsilon}^{-n}(T) \cap \Delta)$ , where  $\Delta$  is, as above, the diagonal.

In addition, since each point  $q \in K_\mu \setminus P(O)$  also has a stable manifold  $W^s(q)$ , with arguments like  $\lambda$ -lemma (see [16]) one can prove that the component of  $W^s(q)$  containing  $q$  is a circle accumulated by the boundaries of the annuli above described. Consequently the complement of  $B_\infty(F_{\mu,\epsilon})$  is a Cantor set of circles; in fact, every pair of points in  $K_\mu$  with same image under  $F_{\mu,\epsilon}$  are joined by such a circle. Observe that this Cantor set of circles is just the closure of  $\bigcup_{n \geq 0} F_{\mu,\epsilon}^{-1}(\Gamma)$ . Right picture in Figure 12 is an illustration of that phenomenon.

**Second way:**  $F_{\mu,\epsilon}^{-1}(T)$  is contained into the interior of  $C_{\mu,\epsilon}$ .

This case is really of higher complexity than the previous one. To facilitate our unfinished attempt to describe how the components of  $B_\infty(F_{\mu,\epsilon}) \cap \text{int } \Gamma$  are arranged we introduce the following concept. An annulus is said to be *large* if each circle in its boundary goes through  $L_1$  and  $L_2$ .

Due to the location of the disk  $F_{\mu,\epsilon}^{-1}(T)$ , two facts follow:

- The preimage of  $F_{\mu,\epsilon}^{-1}(T)$  is disjoint union of four disks, the interior of each disk is part of  $B_\infty(F_{\mu,\epsilon})$ ; further, two of them intersect  $P(O) \setminus \{O, S_1\}$  and the other two have no preimage. Generically these four disk are displayed as illustrated in Figure 13. All pictures in this figure were generated using Option 3.
- Since  $O$  is a hyperbolic saddle, from  $\lambda$ -lemma it follows that if  $A$  is a disk in  $F_{\mu,\epsilon}^{-2}(T)$  intersecting  $\Delta$ , then there exist  $k \geq 1$  and a component  $B$  of  $F_{\mu,\epsilon}^{-k}(A)$  such that  $B$  is a disk whose boundary goes through  $L_1$  and  $L_2$ ; pictures in Figure 14 show this situation for  $\epsilon = 0.38$  and  $\mu = 4.16$  (picture in the left side), and  $\epsilon = 0.3755$  and  $\mu = 4.007$  (picture in the right side). The preimage  $F_{\mu,\epsilon}^{-1}(B)$  is not necessarily a large annulus; indeed, it is generically displayed in one of the three ways as shown in Figure 15; right there the left annulus is the only large; central and right annuli will be called *small* and *singular* annulus, respectively. The preimages of these three type of annuli are displayed of three different manners, from left to right: two annuli, at least one of them large; four annuli, none large; and one annulus minus four disks. An interesting problem is the following:

**Problem.** *In the second way setting, give a detailed description of all manners in which the basin of attraction of  $\infty$  in  $\text{int } \Gamma$  is displayed.*

We advance that among the components of  $B_\infty(F_{\mu,\epsilon}) \cap \text{int } \Gamma$  always there are large and small annuli. Given a large annulus in  $B_\infty(F_{\mu,\epsilon}) \cap \text{int } \Gamma$ , the preimage of its components in  $C_{\mu,\epsilon}$  are two annuli; one of them is large and its components in  $C_{\mu,\epsilon}$  are closer to  $O$  and  $S_1$  than the previous ones. The preimage of the other component may be large, small or singular, it is closer to  $F_{\mu,\epsilon}^{-1}(T)$  than the given annulus. So, from  $\lambda$ -lemma and continuity it follows that  $\Gamma$  is accumulated by large annuli; in fact, it is accumulated by preimages of closer component to  $O$  of large annuli. Consequently the stable manifold of  $O$  is accumulated by preimages of large annuli. It is also clear that the boundary of  $F_{\mu,\epsilon}^{-1}(T)$  is accumulated by small annuli.

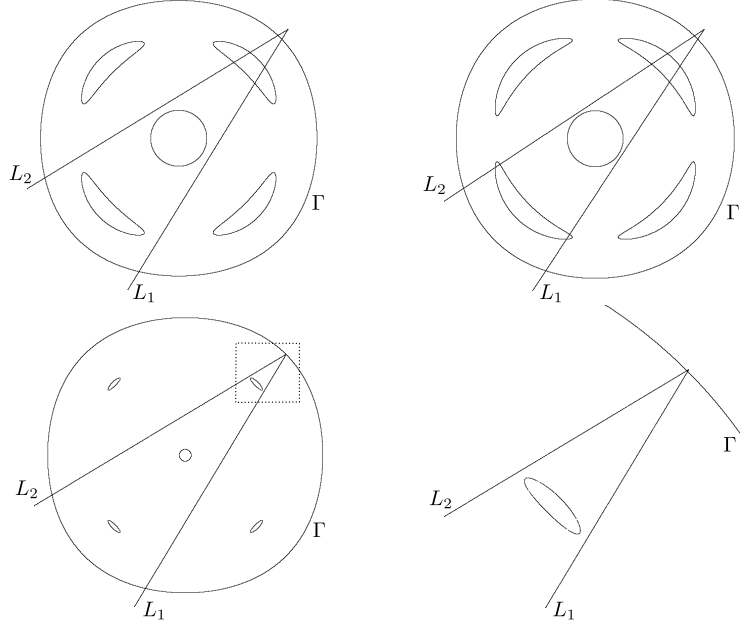


Figure 13: The pictures of the top and the picture in left side of the bottom illustrate the generic configurations of the preimage of  $F_{\mu, \epsilon}^{-1}(T)$  (central disk). In left top picture  $\epsilon = 0.38$  and  $\mu = 4.16$ , in right one  $\epsilon = 0.397$  and  $\mu = 4.16$ ; in left bottom picture  $\epsilon = 0.3755$  and  $\mu = 4.007$ . The picture in the right side of the bottom picture is a magnification of the dotted square.

Observe that in all of these computational simulations  $\mu < \mu_0(\epsilon)$ .

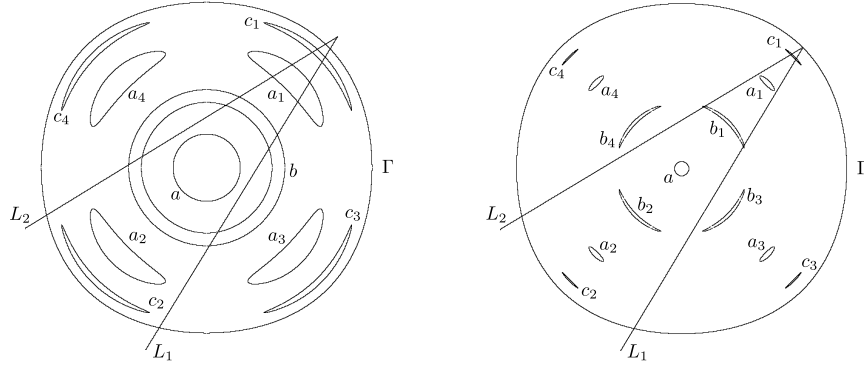


Figure 14: In both picture, the disks denoted by  $a_1, a_2, a_3$  and  $a_4$  are the preimage of  $F_{\mu, \epsilon}^{-1}(T)$  (central disk). The annulus  $b$  in left picture is the preimage of the disk  $a_1$ , and the disks  $b_1, b_2, b_3$  and  $b_4$  constitute the preimage of  $a_1$  in picture on the right side.

On the other hand, observe that the number of disks in  $\bigcup_{n \geq 1} F_{\mu, \epsilon}^{-n}(T)$  is finite. This is consequence of the following facts: those disks in  $\bigcup_{n \geq 1} F_{\mu, \epsilon}^{-n}(T)$  that do not cut  $\Delta$  have no preimage, and among those who cut the diagonal, only two of them are



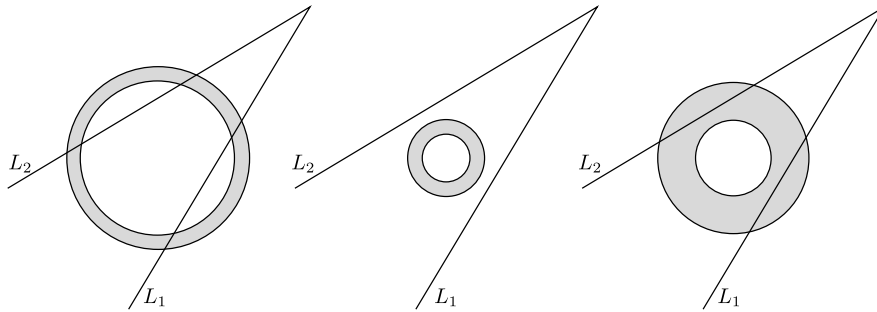


Figure 15: The three generic possibilities for the preimage of a disk whose boundary in  $C_{\mu,\epsilon}$  goes through  $L_1$  and  $L_2$ .

such that the boundary of each one goes through  $L_1$  and  $L_2$ ; one of these two disks is near  $O$  and the other one is near  $S_1$ . The preimage of the first of these disks is a large annulus (as it is known); the preimage of the second one may be a large, small or singular annulus. Suppose it is singular, hence any other annulus surrounding  $F_{\mu,\epsilon}^{-1}(T)$  must be either large or a small annulus. The same thing happens if a singular annulus surrounds any other of the disks above; thus, there can only be a finite number of singular annuli. Figure 16 shows a numerical evidence of the existence of a singular annulus when  $\mu = 4.03$  and  $\epsilon = 0.394$ . Pictures at the top of this figure were obtained with Option 3; in the left picture observe that the annulus denoted by  $a$  is a singular annulus and it is the preimage of the disk indicated with  $b$ . Sector  $d$  (at the right) is the preimage of  $a$ . Picture at the bottom was generated by means of Option 2 with starting point  $(0.1, 0)$ , region in black corresponds to huge numbers of forward and backward iterations of this point.

**3.1.2. Attractors inside  $\text{int } \Gamma$ .** In a wide variety of dynamical systems there are several coexisting attractors, many of them easy to be detected both numerically and theoretically. To fully understand the dynamics of these systems one should identify all the possible attractors and their basins of attractions. At this point the computational simulation is actually an important tool, it allows the location of possible attractors and their basins.

To specify terms we recall that if  $T$  is a continuous self-map on a metric space  $X$ , a compact subset  $A$  of  $X$  is called *attracting set* for  $T$  if  $T(A) \subset A$  ( $A$  is invariant) and there exists a neighborhood  $V$  of  $A$  such that for any neighborhood  $U$  of  $A$  there exists an integer  $n_U$  such that for any  $n > n_U$ ,  $T^n(V) \subset U$ . Observe that for any point  $x \in V$  it holds that  $T^n(x) \rightarrow A$  when  $n \rightarrow +\infty$ . The *basin of attraction* of an attracting set  $A$  is the set of points whose forward orbit accumulates on  $A$ ; clearly the basin of attraction of  $A$  is the equal to  $\bigcup_{n \geq 0} T^{-n}(V)$ . An *attractor* for  $T$  is any attracting set containing a dense forward orbit. We remark that an attracting set may contain one or several attractors. We say that an attracting set is a *fat attractor* if it has positive Lebesgue measure. The term fat attractor is also

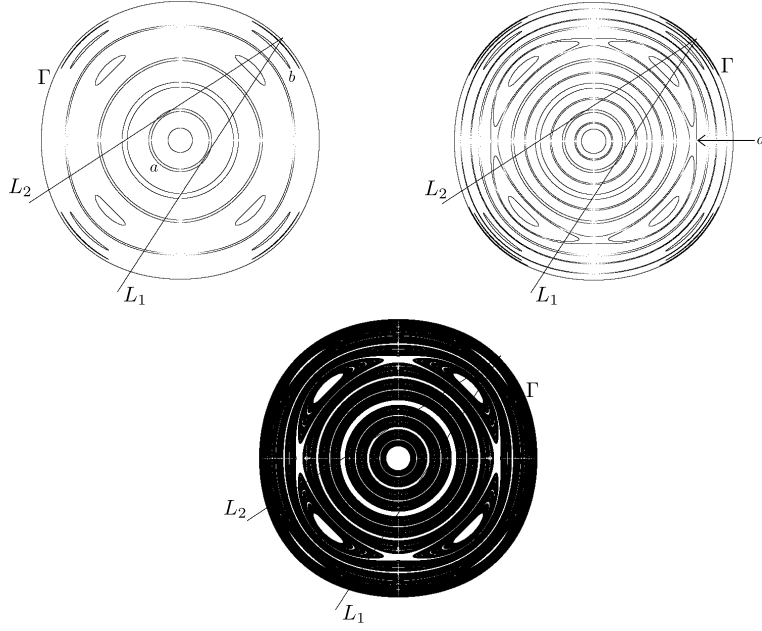


Figure 16: Computational illustration through which the existence of singular annuli is evidenced. White sectors at figure bottom illustrates some components of  $B_\infty(F_{\mu,\epsilon})$ .

used in other settings, see for example [12], [15] and [19]. We refer to [13, 14] for further discussion on the definition of attractors.

In this paragraph we show some numerical evidences of the existence of fat attractors for  $F_{\mu,\epsilon}$ . First, observe that for  $1 < \mu \leq \max\{\mu'(\epsilon), \mu_0(\epsilon)\}$ , there is nothing relevant to say about the forward asymptotic behavior of the orbits starting in  $cl(int \Gamma)$ : the omega limit set of all  $z \in cl(int \Gamma)$  is either contained in  $\{R(p_{\mu,\epsilon}), p_{\mu,\epsilon}\}$  or in the segment  $OS_1$ . Therefore we will consider the following two cases for the parameter regions:  $0 < \epsilon < 3/8$  and  $\mu'(\epsilon) < \mu \leq 4$ , and  $\max\{4, \mu_0(\epsilon)\} < \mu \leq \mu_1(\epsilon)$ ; see Figure 3.

**a) Case 1.**  $0 < \epsilon < 3/8$  and  $\mu'(\epsilon) < \mu \leq 4$ .

From Theorem A it is clear that  $cl(int \Gamma) = B_\infty^c(F_{\mu,\epsilon})$  and  $ext \Gamma = B_\infty(F_{\mu,\epsilon})$ . We believe, according to computational simulations, that in the parameter region above there are sets with positive measure for which  $F_{\mu,\epsilon}$  exhibits fat attractors. A theoretical proof of this statement seems very hard, so we only show several images as numerical evidences of this occurrence.

The first attempt to detect fat attractors is for parameter values close to  $\epsilon = 0$  and  $\mu = 4$ , this is because for these values of  $\epsilon$  and  $\mu$  almost every point inside  $int \Gamma$  has dense orbit in the square  $Q$ . So, for  $\mu \leq 4$  and  $\epsilon > 0$  close enough to 4 and 0 respectively, the map  $F_{\mu,\epsilon}$  should also exhibit fat attractors. Figure 17 shows fat attractors (black regions) when  $\epsilon = 0.01$  and  $\mu$  takes three different values: 4, 3.7 and 3.694. These regions were obtained by plotting a huge number

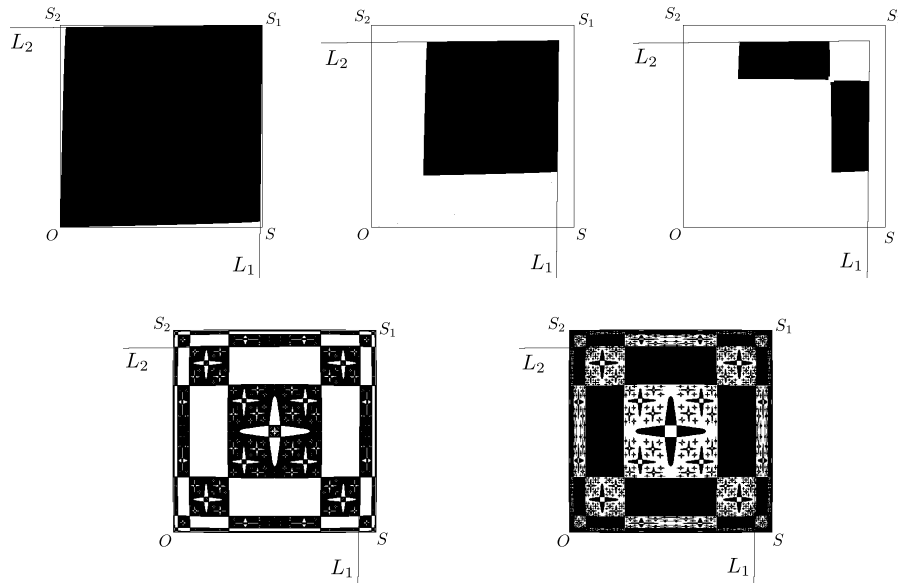


Figure 17: The parameters for the picture in the left side are  $\mu = 4$  and  $\epsilon = 0.01$ , for the central picture  $\mu = 3.7$  and  $\epsilon = 0.01$  and for the right picture  $\mu = 3.694$  and  $\epsilon = 0.01$ ; this last fat attractor is 2-periodic. Pictures in the bottom were obtained through Option 2 to visualize an approximation of the basins of attraction of the attracting set in the segment  $OS_1$  (left picture) and the fat attractor when  $\mu = 3.694$  and  $\epsilon = 0.01$  (right picture).

$(2 \times 10^8)$  of forward iterated of points in the square  $Q$ . For that parameters, the black regions in that figure illustrate the only fat attractors of  $F_{\mu,\epsilon}$ . However there may be other attractors, for example when  $\epsilon = 0.01$  and  $\mu = 3.694$  the map  $F_{\mu,\epsilon}$  has an attractor on the diagonal. We justify this statement through computational simulation. Recall that if one takes any point on the segment  $OS_1$ , then its forward orbit remains in this segment and accumulates on the attractor of the logistic map  $f_\mu$ ; it is obvious that the forward orbit of every point in any preimage set of that point also accumulates on that attractor. Therefore Option 2 is a nice tool to detect the basin of possible attractors. We have done this computational simulation with  $\epsilon = 0.01$  and  $\mu = 3.694$ , the results are the pictures in the bottom of Figure 17.

For other values of the parameters  $\mu$  and  $\epsilon$  there may be more than one fat attractor, this is numerically evidenced in the pictures of Figure 18. The two fat attractors in that figure are located in the left side (bottom and top), pictures in the right side are approximations of the basin of attraction (black sectors) of the corresponding attractor to its left side. Such basins of attraction were obtained by using Option 2 as explained above. Observe that these attracting sets are periodic with period 2 and their basins look complementary, so there are no more attractors when  $\mu = 3.67$  and  $\epsilon = 0.01$ .

To finish with this case we will report some numerical evidences revealing not

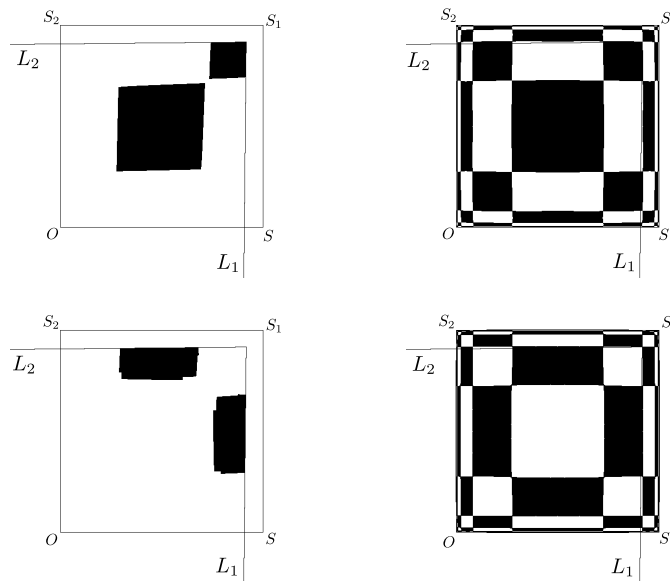


Figure 18: Two different fat attractors for the same map  $F_{\mu, \epsilon}$ , here  $\mu = 3.67$  and  $\epsilon = 0.01$ .

only the existence of fat attractors when  $\mu = 4$  but also the dynamics richness in their evolution. We recall that the logistic map  $f_4$  has the interval  $[0, 1]$  as a completely invariant set and its dynamics is chaotic in Devaney's sense; see [3]. This fact is perhaps not exactly relevant for the following discussion, but it does provides information about the dynamics of  $F_{4, \epsilon}$  restricted to the diagonal. In Figure 17 we have shown a such attracting set for  $\epsilon = 0.01$ , this kind of attracting sets persist when  $\epsilon$  increases at least until  $\epsilon = 0.11$ ; see the fat attractor located in the left side of the top of the Figure 19. The 2-periodic fat attractor to its right side appears when  $0.11 < \epsilon \leq 0.1115$ , in this case  $\epsilon$  is exactly 0.1115; it is a break of the continuum of fat attractors when  $\epsilon > 0$  grows from 0. Clearly this attracting set does not contain the segment  $OS_1$ , which we believe is an attractor. The reason of our belief is based on the fact that by plotting a huge number of preimages of the origin, indeed using Option 2 to any point in  $OS_1$ , the result is a set of points whose complement should be the basin of attraction of that 2-periodic fat attractor; picture at the bottom of Figure 19 shows that plotting set when  $\epsilon = 0.1115$ . To produce the picture in the middle of Figure 19, that is when  $\epsilon = 0.11999$ , we have used Option 0; the result is an apparently diffuse set of points. However, when one does a magnification in on one of its two parts, small fat regions can be observed; just with these regions a periodic fat attractor is constituted: the 2-periodic fat attractor transits by an explosion in its parts to produce a higher order periodic fat attractor, see the zoom of the box in the image mentioned above. After that explosion the pieces of the new periodic fat attractor seem to come together to form a new type of attracting set, Figure 20 shows the state of that evolution when

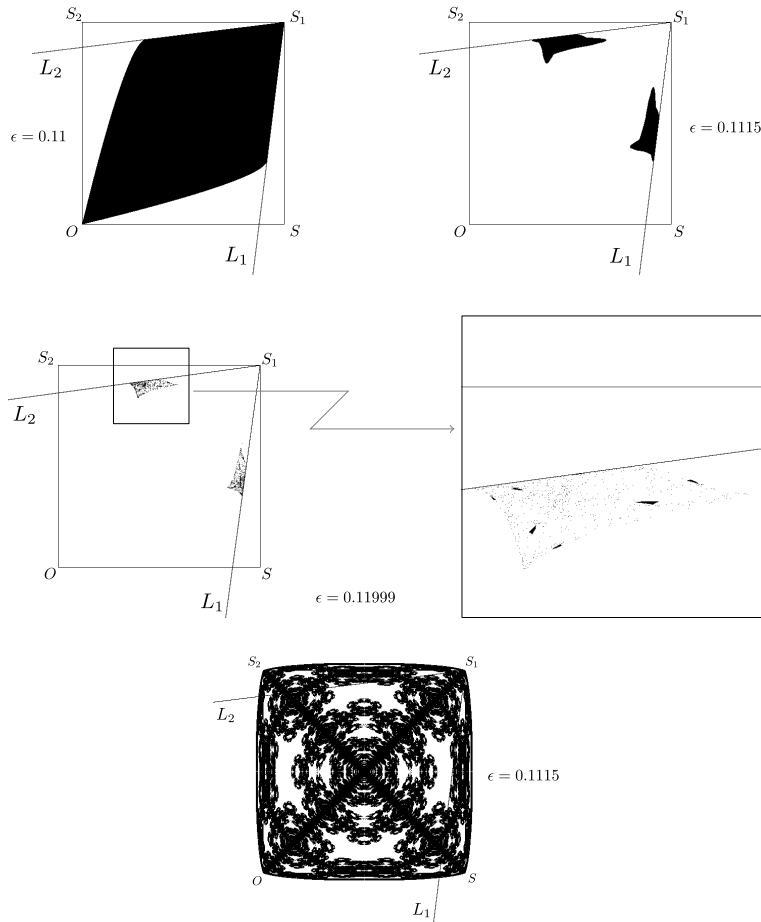


Figure 19: This figure marks the beginning of how fat attractors change when  $\mu = 4$  and  $\epsilon$  grows from 0. Pictures at the top and in the middle were obtained with Option 0, while the image at the bottom was generated with Option 1 applied to the origin, it also can be obtained with Option 2 applied to any point in the segment  $OS_1$ ; sectors in white constitute what seems to be the basin of attraction of the 2-periodic fat attractor at the top.

$\epsilon = 0.125$ . This new 2-periodic attracting set evolves towards two circles that we believe come from a Hopf bifurcation of an attracting 2-periodic orbit. Pictures in Figure 21 show a numerical evidence of this evolution. The attracting 2-periodic orbits in the analytic continuation of the 2-periodic orbit producing that possible Hopf bifurcation are located near  $L_1$  and  $L_2$ , and lose attraction power when  $\epsilon$  increases; we believe that this 2-periodic orbit disappears and even it gives rise to attracting sets that we do not know how to identify or classify.

When  $\epsilon$  is between 0.14 and 0.19 it is relatively easy to detect (by means of computational simulations) an 2-periodic orbit as the attractor of  $F_{4,\epsilon}$  outside the segment  $OS_1$ , as above that segment is an attracting set whose basin is like the

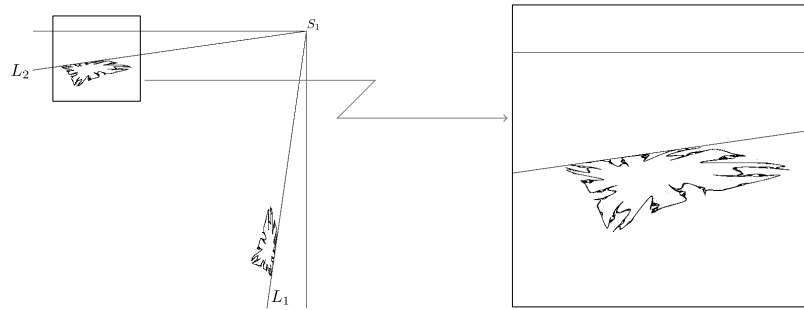


Figure 20: Here the parameters are  $\mu = 4$  and  $\epsilon = 0.125$ , as above it was used Option 0 to produce it. This 2-periodic attractor appears after the explosion of the 2-periodic fat attractor in Figure 19. As for the periodic fat attractors with  $\epsilon = 0.1115$  or  $\epsilon = 0.11999$ , in this case the segment is also an attractor, its basin of attraction is like indicated at the bottom of Figure 19.

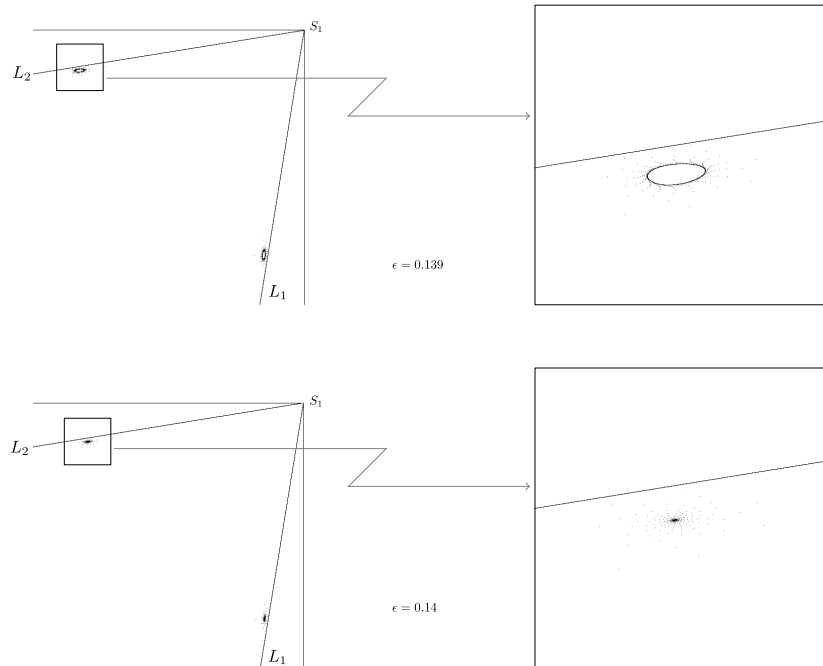


Figure 21: Numerical evidences of the evolution of the fat attractors going through a Hopf bifurcation when  $\epsilon$  increases from 0 and  $\mu = 4$ .

picture at the bottom in Figure 19. For each  $\epsilon$  with  $0.19921 \leq \epsilon \leq 0.25$  is observed a fat attractor containing the segment  $OS_1$ , it is unique for the corresponding value of  $\epsilon$  and it looks like the fat attractor in Figure 19 with  $\epsilon = 0.11$ , but with smaller area. Indeed, it is also numerically observed that when  $\epsilon$  grows that area decreases to zero. This fact forces that the segment  $OS_1$  is just the attracting set of  $F_{4,\epsilon}$  inside  $\text{int } \Gamma$  when  $\epsilon$  varies from the value nulling that area until  $\epsilon = 0.5$ .

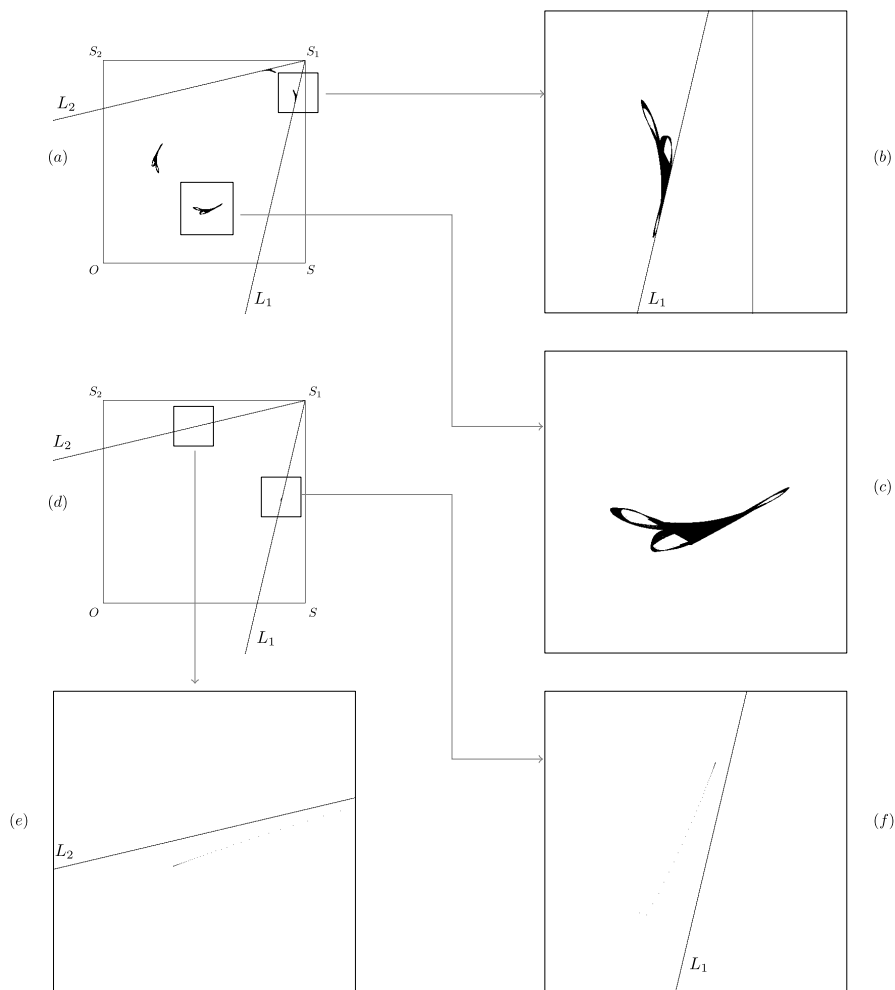


Figure 22: All the pictures in this figure were obtained applying Option 0 with  $\epsilon = 0.1915$  and  $\mu = 4$ . This computational simulation was done with a lot of points, in both cases we select initial conditions whose forward orbit quickly accumulates in the attracting set. The results suggest that there are at least two attracting sets: an 2-periodic orbit (located very near of  $L_1$  and  $L_2$ ) and apparently an 4-periodic fat attractor. The first one is in picture (d), indeed on the computer screen it is not clear to see it, but when magnifying appropriate sectors that orbit is detected; this is showed in pictures (e) and (f). The fat attractor is in picture (a); while (b) and (c) are magnifications of the boxes indicated there.

When  $\epsilon$  transits the interval  $(0.19, 0.19925)$  it is really difficult to say globally something interesting about the attracting sets for  $F_{4,\epsilon}$ . So we only show a few pictures in Figure 22 that are somehow a numerical confirmation of the richness and complexity of the dynamics of that self-map.

**b) Case 2.**  $\max\{4, \mu_0(\epsilon)\} < \mu \leq \mu_1(\epsilon)$

In this case it is clear that the basin of attraction of  $\infty$  always has components inside

$\text{int } \Gamma$ : the triangular region  $T$  described in Remark 2.1 is always present. When the area of that components grows it is even more difficult to detect attracting sets different from  $\infty$ ; indeed that area increases when  $\mu$  grows, which happens if  $\epsilon \nearrow 0.5$ . Thus, we have done some computational simulations with values of  $\mu$  near 4 and  $\epsilon$  near those used to detect attracting sets when  $\mu = 4$ ; therefore it is natural that the attracting sets detected are, in some way, related with the dynamical configuration when  $\mu = 4$ . Take for example  $\epsilon = 0.14$ ; if one increases the value of  $\mu$ , one will observe the (partial) evolution of the 2-periodic orbit detected when  $\mu = 4$ ; see Figure 21. It can be numerically observed that this 2-periodic orbit also transits by a Hopf bifurcation when  $\mu$  grows from 4; our computational simulations report the following results:

- a) When  $4 \leq \mu \leq 4.00411$  the 2-periodic orbit above seems to be the only attracting set of  $F_{\mu,\epsilon}$ ; it is also noticeable the variation of the nature of the eigenvalues associated to that periodic orbit.
- b) When  $\mu$  runs the interval  $[4.00412, 4.05284694]$ , instead of the previous orbit there is an 2-periodic attracting set constituted by two circles; between 4.00411 and 4.00412 a Hopf bifurcation has occurred.
- c) The two circles that emerged from the preceding Hopf bifurcations do not appear when  $\mu = 4.05284695$ , instead there seems to be an attracting periodic orbit with period bigger than 2. This new periodic orbit also looks to travel through a Hopf bifurcation; Figure 23 show the periodic circles that arise after a new possible bifurcation, in this case  $\mu = 4.085$ . These attracting periodic circles also disappear

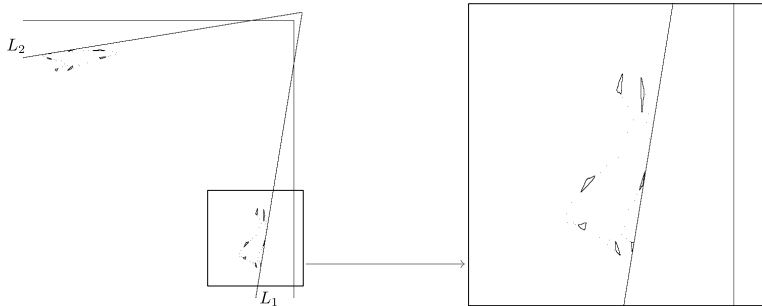


Figure 23: An illustration of the periodic circles that have emerged after a second Hopf bifurcation when  $\mu$  increases from 4 and  $\epsilon = 0.14$ . In this figure  $\mu = 4.085$ .

creating new attracting periodic orbit of even greater period. This process seems to repeat itself until a periodic fat attractor appear. In Figure 24 it is shown such a periodic attracting set, in this case  $\mu = 4.088$ . In some way, of which we have no idea, the pieces on each side of the diagonal of this attracting set connect to each other to form a piece of an 2-periodic fat attractor; this one is shown in Figure 25 for  $\mu = 4.089$ .



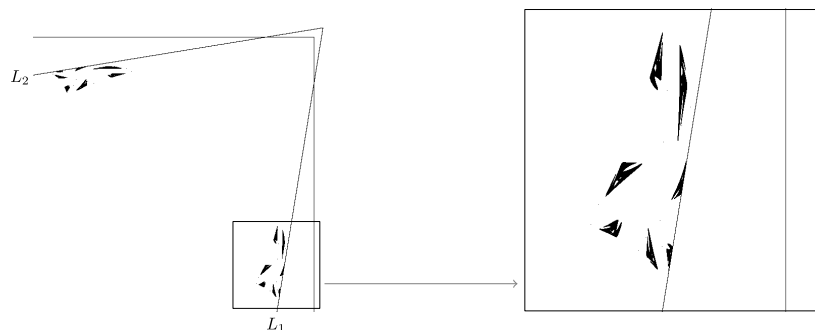


Figure 24: This figure represents the periodic fat attractor that arises after the disappearance of the periodic circles that emerged from the second Hopf bifurcation.

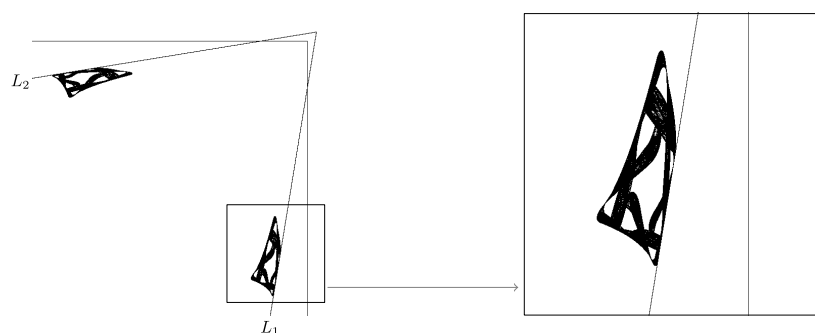


Figure 25: This 2-periodic fat attractor is obtained as a result of the collapse of the pieces (on each side of the diagonal) of the periodic fat attractor in the previous figure.

d) The 2-periodic fat attractors described above are easily detected until  $\mu = 4.1213$ , after this value of  $\mu$  we could not find, even by means a huge number of computational simulations, at least one attracting set. However, an obvious remark: every

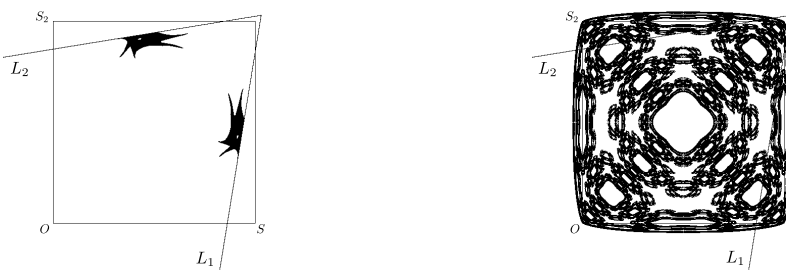


Figure 26: This 2-periodic fat attractor is obtained when  $\epsilon = 0.14$  and  $\mu = 4.1213$ , to its right side is a graphical representation of a huge number of preimages of  $O$ , which distinguishes the components of the basin of that attracting set and the components of  $B_{\infty}(F_{\mu, \epsilon})$ .

point in  $cl(int \Gamma) \cap cl(C_{\mu, \epsilon})$  has bounded orbit, hence it has non-empty omega limit set, and this does not imply that there are attracting sets inside  $int \Gamma$ . In Figure 26 we show two pictures, both with  $\epsilon = 0.14$  and  $\mu = 4.1213$ ; the picture in the left side is the 2-periodic fat attractor referred above, it was obtained (as always) by using Option 0. The other one is the result of plotting of a large number of preimages of the origin, its exterior border is an approximation of  $\Gamma$ , the white sectors correspond to: the components of  $B_{\infty}(F_{\mu, \epsilon})$  inside  $int \Gamma$ , and the components of the basin of attraction of the 2-periodic fat attractor.

**3.1.3. Invariant curves beyond  $\epsilon \mapsto \mu_1(\epsilon)$ .** As announced at the end of item 2 in Remark 2.1, we have no a proof for the existence of the curve  $\Gamma$  (as introduced in Theorem A) when  $\mu > \mu_1(\epsilon)$  and it is close to  $\mu_1(\epsilon)$ ; however, there we discussed

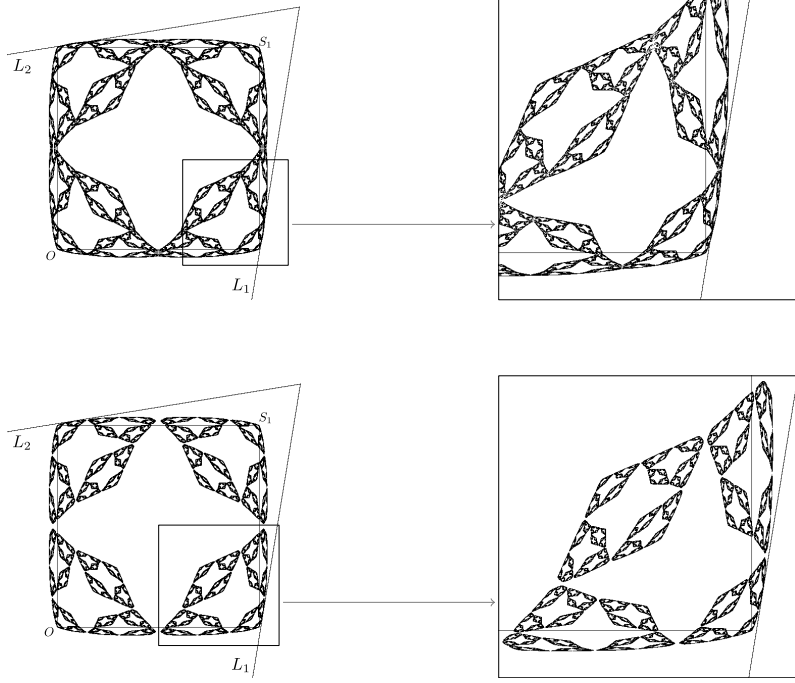


Figure 27: For the pictures at the top we have used  $\epsilon = 0.14$  and  $\mu = 4.8$ , they show an invariant curve  $\Gamma$  beyond  $\epsilon \mapsto \mu_1(\epsilon)$ ; while for the pictures in lower part  $\epsilon = 0.14$  and  $\mu = 4.82$ , with these values there is no curve as stated in Theorem A.

some ideas of how such a proof could be made. Pictures at the top of Figure 27 numerically show, for  $\epsilon = 0.14$  and  $\mu = 4.8$ , the existence of a positively invariant curve  $\Gamma$  (exterior border of picture in the left side) such that  $ext \Gamma$  is the immediate basin of attraction of  $\infty$ . For in this computational simulation the point  $S$  is in the interior of the cone  $C_{\mu, \epsilon}$ ; that is  $\mu > \mu_1(\epsilon)$ , see the magnification of the box in the picture located in the upper left corner. At this time we consider appropriate to establish the following conjecture:

**Conjecture:** *If  $\epsilon \in (0, 1/2)$  and  $\mu > 1$  satisfy  $\mu > \mu_1(\epsilon)$  and there exists a curve  $\Gamma$  as in Theorem A, then  $B_\infty^c(F_{\mu,\epsilon})$  is the closure of  $\bigcup_{n \geq 0} F_{\mu,\epsilon}^{-n}(\Gamma)$ .*

In the small strength case, the computational simulations reveal that there is always an invariant curve  $\Gamma$  as in Theorem A whenever  $\mu > \mu_1(\epsilon)$  and close enough to  $\mu_1(\epsilon)$ . We would like to recall that this curve disappears when the value of  $\mu$  grows, this certainly occurs when from a certain preimage of the circle  $C$ , the following ones are inside  $C_{\mu,\epsilon}$ . In this case the basin of attraction  $B_\infty(F_{\mu,\epsilon})$  is again connected and its complement has infinitely many components. It is well known that this last set is an expanding Cantor set for all  $\mu$  large enough, see [18].

**3.2. Large strength case.** The aim of this part is analagous to that of the subsection 3.1. In this setting it is well known that if  $\mu$  and  $\epsilon$  satisfy  $1 < \mu \leq \mu'_0(\epsilon)$ , then the set of points with bounded orbit is the union of the segments  $OS_1$  and  $SS_2$ ; in addition, the forward orbit of every  $z$  in this union converges to the fixed point  $P_\mu = (\frac{\mu-1}{\mu}, \frac{\mu-1}{\mu})$ . On the other hand, if  $1 < \mu \leq \mu_1(\epsilon)$ , then the phenomenon of Cantor's set of circles discussed in the small straight case is not possible, this is due to the absence of a Cantor set on the diagonal.

**3.2.1. Attractors inside  $int \Gamma$ .** As in the small strength case, there are regions in the parameter space with  $1 < \mu \leq \mu_1(\epsilon)$  where the map  $F_{\mu,\epsilon}$  exhibits fat attractors when  $\mu$  and  $\epsilon$  are near 4 and 0, respectively. In order to not to be repetitive we do not show such examples; however, we will show some type of attracting sets that we did not exhibit before.

Take  $\epsilon = -0.9$ , so  $\mu_1(\epsilon) \sim 2.714$  and  $\mu_2(\epsilon) \sim 2.357$ . For  $\mu = 2.71$  the map  $F_{\mu,\epsilon}$  has the fat attractor plotted in Figure 28 (left picture). This attractor has

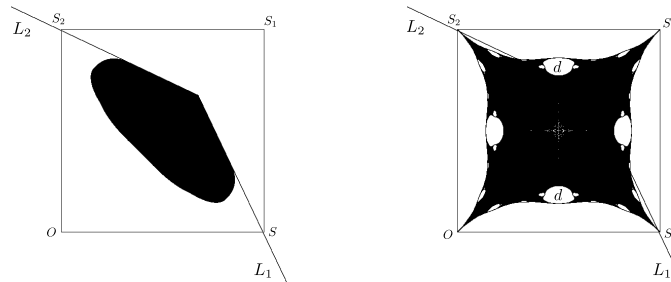


Figure 28: Fat attractor (left picture) and its basin (right picture) when  $\epsilon = -0.9$  and  $\mu = 2.71$ .

been generated applying Option 0 to the point  $(0.67, 0.59)$ , just with this point and Option 2 one obtains an illustration of the basin of that attractor; see picture on the right side in Figure 28. Observe that the exterior border of that picture is an approximation of the Jordan curve  $\Gamma$ . We take advantage of it to reiterate the existence of components (white regions) of  $B_\infty(F_{\mu,\epsilon})$  inside  $int \Gamma$ , this was discussed in item 2 of Remark 2.2. Recall that there exists only one way to produce these components in the large strength case. In Figure 29 we show a magnification of a

neighborhood of the point  $S$  where it can be seen an arc of  $\Gamma$  through which are produced the two components of  $B_\infty(F_{\mu,\epsilon})$  indicated by  $d$  in the picture in the right side of Figure 28.

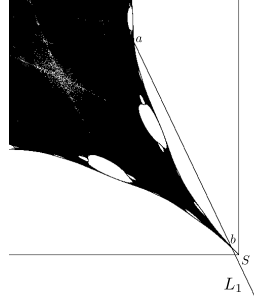


Figure 29: The sector whose boundary is given by the segment  $ab$  in  $L_1$  and the arc in  $\Gamma$  between the points  $a$  and  $b$  produces some components of  $B_\infty(F_{\mu,\epsilon})$  intersecting the critical line  $\ell_1$ .

Try to explain, even to understand, how the fat attractor in Figure 28 evolved when  $\mu$  varies and  $\epsilon$  stays equal is a very hard task. In the following pictures we present some numerical experiments, with  $\epsilon = -0.9$ , which partially show the possible attractors of  $F_{\mu,\epsilon}$  inside  $\text{int } \Gamma$ . In that picture sequence the parameter  $\mu$  takes some values in the interval  $(\mu_2(\epsilon), \mu_1(\epsilon))$  in an increasing way. We recall that if  $\mu \in (\mu'_0(\epsilon), \mu_2(\epsilon)]$ , the fixed point  $P_\mu$  is the only attractor of  $F_{\mu,\epsilon}$  inside  $\text{int } \Gamma$ . It is important to say that these numerical experiments have been repeated for a large number of values of  $\epsilon < 0$  and similar figures or attractors have been observed to those shown in Figure 30. In the picture corresponding to  $\mu = 2.37$  it is observed as attractor an 2-periodic orbit. From the numerical point of view, this dynamical configuration remains for a certain range of values of  $\mu$  in which the nature of the eigenvalues associated to that periodic orbit evolves towards a Hopf bifurcations, which should occur for some  $2.525 < \mu < 2.53$ . The picture associated to  $\mu = 2.525$  induces to think that the eigenvalues of the 2-periodic orbit are non-real with negative real part; the picture corresponding to  $\mu = 2.53$  shows the 2-periodic attracting circles generated by that Hopf bifurcation. These two circles go through a degenerative stage losing differentiability, approaching to the boundary of  $C_{\mu,\epsilon}$  until they disperse in a cloud of points (perhaps a periodic orbit of very large period) to later constitute a fat periodic attractor; this part of the evolution is briefly illustrated in the pictures corresponding to  $\mu = 2.59$ ,  $\mu = 2.61$  and  $\mu = 2.6157$ . Finally, the pictures associated to  $\mu = 2.62$ ,  $\mu = 2.67$  and  $\mu = 2.68$  show the collapse of that fat periodic attractor in a single one, gaining area until reaching the fat attractor in Figure 28.

**3.2.2. Invariant curves beyond  $\epsilon \mapsto \mu_1(\epsilon)$ .** In the large strength case when  $\mu_1(\epsilon) < \mu < 4$  the preimage of  $\partial Q$  continues to be a closed curve joining the points in  $F_{\mu,\epsilon}^{-1}(O)$ ; so it is still possible to discuss the existence of a forward invariant Jordan curve containing  $F_{\mu,\epsilon}^{-1}(O)$ ; see item 3 of Remark 2.2. However, one can not hope

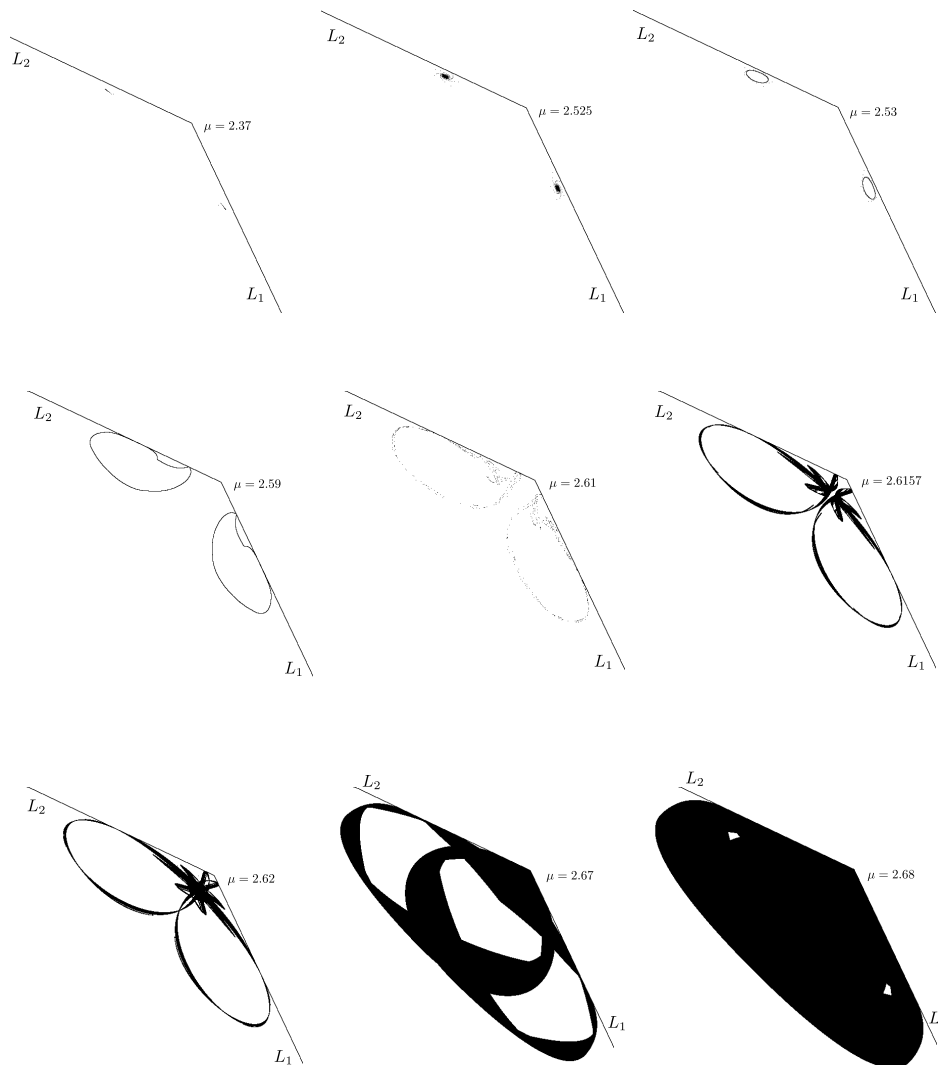


Figure 30: A simplistic and inaccurate graphical illustration of the evolution towards the fat attractor in Figure 28.

neither differentiability of the arcs  $\Gamma_b, \Gamma_\ell, \Gamma_r$  and  $\Gamma_t$  of  $\Gamma$ , nor  $ext\Gamma \subset B_\infty(F_{\mu,\epsilon})$ ; pictures in Figure 31 are numerical samples of these possible features. Since the points  $S$  and  $S_2$  have preimages, we have used Option 1 (applied to the origin) to produce that pictures; notice that their exterior borders look like non-smooth closed curves. In the picture on the right side it can be seen that the preimage of the set indicated with the letter  $a$  contains points with bounded orbits, which belong to the set indicated with  $b$ ; recall what was discussed at the end of item 3 in Remark 2.2.

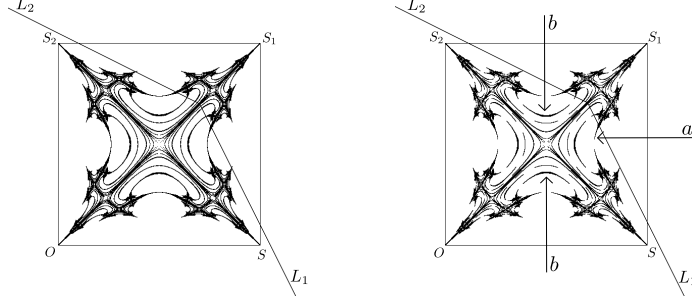


Figure 31: Picture on the left side was generated with  $\epsilon = -1$  and  $\mu = 2.8$ , while the one on the right side was obtained with  $\epsilon = -1$  and  $\mu = 2.82$ .

Now we discuss the special case  $\mu = 4$ . Observe that the square  $Q$  is contained in the interior of  $C_{\mu,\epsilon}$  except by the point  $S_1$ , which is just the vertex of that cone; so, if there exists an invariant Jordan curve  $\Gamma$  as described in Theorem B, then there are no components of  $B_{\infty}(F_{\mu,\epsilon})$  inside  $\text{int } \Gamma$ . Also observe that the preimage of  $Q$  is union of four compact set  $Q_i$  ( $i = 0, 1, 2, 3$ ) such that  $Q_i \cap Q_j = \{(1/2, 1/2)\}$  for all  $i \neq j$ . In particular  $F_{\mu,\epsilon}^{-1}(\partial Q)$  is the union of four closed curves, one for each point in  $F_{\mu,\epsilon}^{-1}(O)$  and having  $(1/2, 1/2)$  as the only common point; pictures in Figure 32 show  $F_{\mu,\epsilon}^{-1}(\partial Q)$  and  $F_{\mu,\epsilon}^{-2}(\partial Q)$ , which were obtained with Option 4 and  $\epsilon = -1$ . It

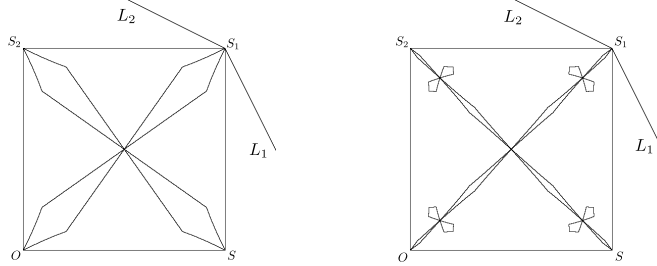


Figure 32: These pictures represent the two first preimages of  $\partial Q$  when  $\epsilon = -1$ . They are similar for all negative value of  $\epsilon$ .

is clear that one can repeat the procedure discussed in item 3 of Remark 2.2 to construct a curve  $\Gamma$ . Another way to achieve the same goal is to resort to the tools that the Iterated Function Systems theory ([1], [8]) provides. The corresponding iterated function system acts on the compact metric space  $Q$  and it is given by the four inverse branches  $H_i$  ( $i = 0, 1, 2, 3$ ) of  $F_{\mu,\epsilon}$ , which are defined by means of (2.1). The aim of this procedure is to show that the iteration of the Hutchinson operator related to that iterated function system converges to a unique attractor: the curve  $\Gamma$ . This property is satisfied if, for example, each self-map  $H_i : Q \rightarrow Q$  is such that one of its iterated is a contraction, a task that in this case looks a bit difficult.

In any case, in the following figure we show an approximation of  $B_\infty^c(F_{\mu,\epsilon})$  when  $\epsilon = -1$ ; it has been produced plotting a huge number of preimages of the origin. We highlight that this self-similar fractal set is analogous to that generated by the same numerical experiment with any value of  $\epsilon < 0$ .

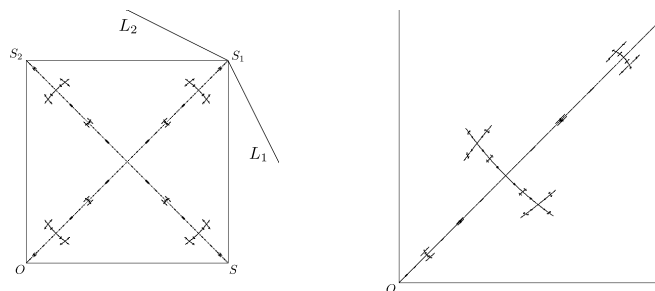


Figure 33: Illustration of the self-similar fractal set representing the set of points with bounded orbits when  $\mu = 4$ . Picture on the right side is a zoom near the origin.

**Acknowledgments.** This research was supported by Grant 002-CT-2015 from the Consejo de Desarrollo Científico, Humanístico y Tecnológico (CDCHT) of the Universidad Centroccidental Lisandro Alvarado.

#### REFERENCES

- [1] M. F. Barnsley and S. Demko. Iterated Function Systems and the Global Construction of Fractals. *Proc. R. Soc. Lond. A* **399**, 243–275 (1985).
- [2] L. A. Bunimovich. Coupled Map Lattices: at the Age of Maturity, *Lect. Notes Phys.* **671**, 9–32 (2005).
- [3] R. Devaney. *An Introduction to Chaotic Dynamical Systems*. Addison-Wesley, 2nd Edition. (1988).
- [4] V. Dobryn'skiy. On properties of coupled quadratic mappings. *Nonlinear Anal.* **35**, 247–267 (1999).
- [5] V. Dobryn'skiy. Critical sets and properties of endomorphisms built by coupling of two identical quadratic mappings. *J. Dynam. Control Systems.* **5**, 227–254 (1999).
- [6] B. Fernandez and M. Jiang. Coupling two unimodal mapas with simple kneading sequences. *Ergod. Th. & Dynam. Sys.* **24**, 107–125 (2004).
- [7] I. Frøyland. Some symmetric, two-dimensional, dissipative maps. *Physica D.* **8**, 423–434 (1983).
- [8] J. Hutchison. Fractals and Self-Similarity. *Indiana Univ. Math. J.* **30**, 713–747 (1981).
- [9] K. Kaneko. Similarity structure and scaling property of the period-doubling phenomena. *Progr. Theoret. Phys.* **69**, 403–414 (1983).
- [10] K. Kaneko. *Theory and Applications of Coupled Map Lattices (Nonlinear Science: Theory and Applications)*. John Wiley & Sons, New York (1993).
- [11] P. Lind, *Pattern Formation in Diffusive-Avective Networks of Discrete-Time Oscillators*. PhD Thesis, University of Lisbon (2003).
- [12] A. O. Lopes and E. R. Oliveira. *On the thin boundary of the fat attractor*. Modeling, Dynamics, Optimization and Bioeconomics III. A. A. Pinto and D. Zilberman (eds.) Springer Proceedings in Mathematics & Statistics **224**, 205 – 246 (2018).
- [13] J. Milnor. On the Concept of Attractor. *Commun. Math. Phys.* **99**, 177–195 (1985).

- [14] J. Milnor. On the Concept of Attractor: Corrections and Remarks. *Commun. Math. Phys.* **102**, 517–519 (1985).
- [15] L. Mora. Homoclinic bifurcations, fat attractors and invariant curves. *Discrete Contin. Dyn. Syst. Ser. A* **9(5)**, 1133–1148 (2003).
- [16] J. Palis Jr. and W. De Melo. *A geometrical introduction to dynamical systems*. Springer (1982).
- [17] N. Romero, J. Silva and R. Vivas. On a coupled logistic map with large strength. *J. Math. Anal. Appl.* **415**, 346–357 (2014).
- [18] N. Romero, A. Rovella and R. Vivas. Invariant manifolds and synchronization for coupled logistic maps. *Int. J. Pure Appl. Math. Sci.* **4**, 39–57 (2007).
- [19] M. Tsujii. Fat solenoidal attractors. *Nonlinearity* **14** 1011 – 1027 (2001).

UNIVERSIDAD CENTROCCIDENTAL LISANDRO ALVARADO. DEPARTAMENTO DE MATEMÁTICA. DECANATO DE CIENCIAS Y TECNOLOGÍA. APARTADO POSTAL 400. BARQUISIMETO, VENEZUELA.  
*E-mail address:* `nromero@ucla.edu.ve`

UNIVERSIDAD CENTROCCIDENTAL LISANDRO ALVARADO. DEPARTAMENTO DE MATEMÁTICA. DECANATO DE CIENCIAS Y TECNOLOGÍA. APARTADO POSTAL 400. BARQUISIMETO, VENEZUELA.  
*E-mail address:* `jesus.silva@ucla.edu.ve`

UNIVERSIDAD NACIONAL EXPERIMENTAL POLITÉCNICA ANTONIO JOSÉ DE SUCRE. VICERRECTORADO DE BARQUISIMETO. DEPARTAMENTO DE ESTUDIOS BÁSICOS. SECCIÓN DE MATEMÁTICA. BARQUISIMETO, VENEZUELA.  
*E-mail address:* `ramon.alberto.vivas@gmail.com`